2017-07-01

Quick Shear Testing of Aggregate Base Materials Stabilized with Geogrid

Rawley Jack Selk
Brigham Young University

Quick Shear Testing of Aggregate Base Materials Stabilized with Geogrid

Rawley Jack Selk

A thesis submitted to the faculty of
Brigham Young University
in partial fulfillment of the requirements for the degree of

Master of Science

W. Spencer Guthrie, Chair
Mitsuru Saito
John D. Hedengren

Department of Civil and Environmental Engineering

Brigham Young University

ABSTRACT

Quick Shear Testing of Aggregate Base Materials Stabilized with Geogrid

Rawley Jack Selk
Department of Civil and Environmental Engineering, BYU
Master of Science

The objective of this research was to apply a previously recommended laboratory testing protocol to specific aggregate base materials that are also the subject of ongoing full-scale field testing. The scope of this research involved three aggregate base materials selected from three sites where full-scale field testing programs have been established. The first and second field sites included five different geogrid types, categorized as either biaxial or triaxial, in a single-layer configuration, while the third site included only the triaxial geogrid type in either a single- or double-layer configuration.

Geogrid-stabilized and unstabilized control specimens were evaluated using the American Association of State Highway and Transportation Officials T 307 quick shear testing protocol. Measurements of load and axial displacement were recorded and used to develop a stress-strain plot for each specimen tested. The peak axial stress, the modulus to the peak axial stress, the modulus of the elastic portion of the curve, and the modulus at 2 percent strain were then calculated. Statistical analyses were performed to investigate differences between geogrid-stabilized specimens and unstabilized control specimens and to investigate differences between individual geogrid products or geogrid configurations.

Depending on the method of data analysis, the quick shear test results indicate that geogrid stabilization, with the effect of geogrid stabilization averaged across all of the geogrid products evaluated in this study, may or may not improve the structural quality of the aggregate base materials evaluated in this study. The results also indicate that, regardless of the method of analysis, one geogrid product or configuration may be more effective than another at improving the structural quality of a given aggregate base material as measured using the quick shear test. All results from this research are limited in their application to the aggregate base material types, geogrid products, and geogrid configurations associated with this study.

Additional research is needed to compare the results of the laboratory quick shear testing obtained for this study with the structural capacity of the geogrid-stabilized and unstabilized control sections that have been constructed at corresponding full-scale field testing sites. Specifically, further research is needed to determine which method of laboratory data analysis yields the best comparisons with field test results. Finally, correlations between the results of quick shear testing and resilient modulus need to be investigated in order to incorporate the findings of the quick shear test on geogrid-stabilized base materials into mechanistic-empirical pavement design.

Key words: aggregate base materials, biaxial geogrid, mechanistic-empirical pavement design, modulus, quick shear test, triaxial geogrid

ACKNOWLEDGEMENTS

This research could not have been accomplished through my efforts alone, and I would be remiss if I did not take this opportunity to make a few specific acknowledgements. I thank Tensar International Corporation and the Utah Department of Transportation for co-sponsoring this project. I also thank several specific students in the Materials and Pavements Research Group at Brigham Young University who were integral in the realization of this research. Jaren Knighton performed precursory research, contributed to Chapters 1 and 2, and was an invaluable resource throughout various stages of the research process. Eric Sweat collected the aggregate base materials from the Orem and Springville field sites, performed washed sieve analyses, and contributed to Chapter 3. Shaun Hilton collected the aggregate base material from the Wells Draw Road field site and assisted with washed sieve analysis and Atterberg limits testing. Kirk Jackson contributed to Chapter 3. Alec Escamilla helped extensively with the laboratory testing. I appreciate Dr. Mitsuru Saito and Dr. John D. Hedengren for participating as members of my graduate committee. I am extremely grateful to my advisor and friend, Dr. W. Spencer Guthrie, for allowing me the opportunity of researching with him. He is a man of many talents who has taught me the importance of professionalism, integrity, and having a passion for work. My wife, Lindsay, for being the one to inspire me to think seriously about graduate school, perhaps deserves the most credit of all. Without her ambitious example, I likely would have let this amazing experience pass by.

TABLE OF CONTENTS

LIST OF TABLES

LIST OF FIGURES

1 INTRODUCTION

1.1 Problem Statement

Flexible pavements are generally designed to have multiple layers, including an asphalt surface course and an aggregate base course over the native subgrade. In pavement design, engineers need to know the structural properties of each layer in order to determine thicknesses of the asphalt and aggregate base layers. For aggregate base materials, structural capacity is commonly quantified in terms of modulus, which is an especially important input in the Mechanistic-Empirical Pavement Design Guide (MEPDG) (AASHTO 2008, NCHRP 2004a, NHI 2002). The modulus of aggregate base layers can potentially be increased through the use of geogrid, an extruded polypropylene material, which would then enable reductions in base layer thickness (Montanelli et al. 1997, Cancelli and Montanelli 1999) and/or prolonged service life (Al-Qadi et al. 1997, Cancelli and Montanelli 1999) compared to unstabilized sections.

Geogrid is available globally in different geometries from several manufacturers, with two primary examples shown in Figure 1-1. Manufactured in wide rolls, geogrid is generally placed directly on prepared subgrade soil or aggregate layers and covered with additional aggregate material that is compacted in place (Montanelli et al. 1997). To the extent that the aggregate particles penetrate the openings, or apertures, in the geogrid, the geogrid increases the lateral confinement of the base material in the region around the geogrid (Al-Qadi et al. 2008,

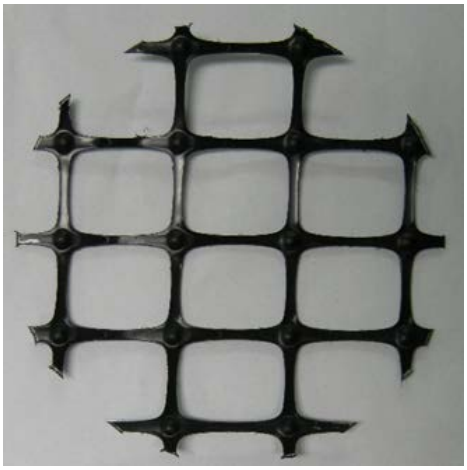

(a)

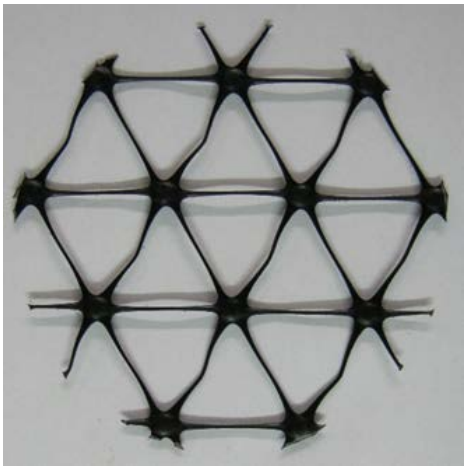

(b)

Figure 1-1: Examples of (a) biaxial and (b) triaxial geogrid.

Qian et al. 2013), which can result in an increase in the modulus of the base layer (Kwon et. al 2008, Perkins 1999, Perkins and Ismeik 1997). In this way, the degree of improvement in modulus is determined by the extent of interlock that occurs between the aggregate and the geogrid; for this reason, geogrid properties such as rib size, aperture size, aperture shape, material type, and tensile strength can influence the interlock that occurs with a given base material (Hatami et al. 2012, Tutumluer and Kwon 2006). Although previous research has been performed to identify laboratory testing protocols that can be used to quantify the expected structural benefit from a given geogrid product for a given aggregate base material (Knighton 2015), additional research is needed to verify the results of the previous testing by comparing laboratory results with those obtained from field testing of the same aggregate base materials and geogrid products. Specifically, laboratory testing is needed for aggregate base materials and geogrid products used at three field sites that were established in previous research (Hilton 2017, Sweat 2016). The present work is intended to support a future comparison of laboratory test results with field test results following completion of the ongoing field testing; the comparison

will show whether laboratory test results can be used to predict the expected benefits of incorporating geogrid into pavement structures in the field.

1.2 Research Objective and Scope

The objective of this research was to apply a previously recommended laboratory testing protocol (Knighton 2015) to specific aggregate base materials that are also the subject of ongoing full-scale field testing. The scope of this research involved three aggregate base materials selected from three sites where full-scale field testing programs have been established. The first and second field sites included five different geogrid types, categorized as either biaxial (BX) or triaxial (TX), in a single-layer configuration (Sweat 2016), while the third site included only the TX geogrid type in either a single- or double-layer configuration (Hilton 2017). To ensure a direct comparison between laboratory and field test results, the same geogrid products that were used at the field sites were also used in the laboratory testing. Furthermore, similar to the field testing, laboratory testing of geogrid-stabilized specimens and unstabilized control specimens was also performed. The laboratory test method that was employed in this research was the quick shear portion of the American Association of State Highway and Transportation Officials (AASHTO) T 307 (Determining the Resilient Modulus of Soils and Aggregate Materials). Following the testing, two statistical analyses were performed on each result of the laboratory testing for each of the three aggregate base materials included in this research. One analysis was performed to investigate differences between geogrid-stabilized specimens and unstabilized control specimens, without distinguishing among geogrid products or geogrid configurations, while the other was performed to investigate differences between individual geogrid products or geogrid configurations. (The intent of the second analysis was not to suggest that a given geogrid

product is generally better than another but rather to investigate the differences in compatibility of the different geogrid products with the specific aggregate base materials included in this research.)

1.3 Outline of Report

This report is divided into five chapters. Chapter 1 introduces the research topic, and Chapter 2 provides background information on geogrid stabilization. Chapter 3 explains the research procedures, and Chapter 4 presents the results and analysis associated with the testing. Finally, Chapter 5 provides conclusions and recommendations based on this research.

2 BACKGROUND

2.1 Overview

This chapter discusses pavement design and construction, gives a brief description of geogrids, and describes geogrid stabilization in the context of both laboratory and field testing of aggregate base materials.

2.2 Pavement Design and Construction

Flexible pavements are generally designed to have multiple layers of varying mechanical properties, with stronger layers placed over weaker layers. The surface course in a flexible pavement structure is normally a hot mix asphalt layer. Having a comparatively high modulus, the asphalt protects the underlying base course and subgrade by decreasing the magnitude of traffic-induced stresses that are transferred downwards into the pavement structure.

The base course is normally composed of a dense-graded aggregate base material, which provides additional protection to the underlying subgrade. Traffic loads are distributed through the base layer through interparticle friction between aggregates (Kwon and Tutumluer 2009, Xiao et al. 2012). As the aggregate base material is compacted in place to a specified density, the resulting interparticle friction, especially between the larger aggregates, allows the base layer to spread traffic loads over the subgrade.

The subgrade is the natural soil that exists on a site and may exhibit very low modulus values. In particular, weak subgrade materials can cause difficulty in road construction because they may not offer sufficient support for compaction of overlying base materials to an appropriate density. For this reason, geogrid reinforcement is sometimes placed over weak subgrades to potentially create an improved construction platform that leads to better compaction and greater strength of the base material (Tutumluer and Kwon 2006, Wayne et al. 2011a).

2.3 Geogrid Description

Geogrid is a high-strength extruded geosynthetic material consisting of connected sets of tensile ribs with apertures that can be penetrated by surrounding aggregate particles (Aran 2006, Reck 2009). Characteristics of geogrid differ due to varying geometric, mechanical, and durability properties (Hanes Geo Components 2015, Tensar International Corporation 2015). Geometric properties include aperture shapes and sizes along with rib spacing, depth, width, length, and shape. Biaxial geogrids, which have rectangular aperture shapes, provide tensile strength in two directions, while triaxial geogrids, which have triangular aperture shapes, provide tensile strength in three directions. The aperture size directly determines the degree to which aggregate particles can penetrate the geogrid. A general recommendation is that the minimum aperture size of the geogrid should be at least equal to the particle size corresponding to 50 percent passing (D_{50}) of the aggregate being placed on the geogrid, but not less than 0.5 in. (13 mm), and the maximum aperture size should be less than or equal to twice the particle diameter corresponding to 85 percent passing (D_{85}), but not greater than 3 in. (76 mm) (FHWA 2008). Mechanical properties include tensile strength, radial stiffness, aperture stability, and flexural rigidity of the geogrid. Durability is a measure of the resistance of geogrid to ultraviolet

degradation, installation damage, and chemical damage (Hanes Geo Components 2015, Tensar International Corporation 2015).

2.4 Geogrid Stabilization

Many field and laboratory studies regarding geogrid stabilization and pavement performance have been conducted to investigate the benefits of geogrid-stabilized aggregate base materials in flexible pavements (Al-Qadi et al. 2008, Haas et al. 1988, Huntington and Ksaibati 2000, Kwon and Tutumluer 2009, Tingle and Jersey 2009). Although the general consensus is that geogrid can be beneficial, quantifying the effect of including geogrid stabilization in pavement structures has proven to be difficult (Aran 2006, Hall et al. 2004). The results of both laboratory and field testing are summarized in the following sections.

2.4.1 Laboratory Testing

Numerous laboratory experiments have been performed to better understand geogrid stabilization of aggregate base material. The experiments involved evaluation of modulus and permanent deformation as measured in the plate load test, triaxial shear test, and repeated load triaxial (RLT) test.

Cyclic plate load testing involves compressive loading of a circular plate and measurement of the surface deflection of the supporting material as described in American Society for Testing and Materials (ASTM) D1195 (Standard Test Method for Repetitive Static Plate Load Tests of Soils and Flexible Pavement Components, for Use in Evaluation and Design of Airport and Highway Pavements). In one study, the results of cyclic plate load tests on laboratory-scale pavement sections with a crushed limestone aggregate base were analyzed using

the MEPDG, and the researchers concluded that geogrid stabilization increased the resilient modulus of the base materials by 10 to 90 percent and suggested that the base layer thickness could therefore be decreased by up to 49 percent (Chen and Abu-Farsakh 2012); in this study, geogrid was placed at one of three locations, including the base-subgrade interface, the middle of the base layer, or the upper one-third position within the base layer in the stabilized sections, which were composed of a 12-in.-thick (305-mm-thick) base layer and a 0.75-in.-thick (19-mm-thick) asphalt layer. However, in another study, cyclic plate load tests performed on crushed base material composed of reclaimed asphalt pavement (RAP) and recycled concrete aggregate (RCA) showed that, while permanent deformation was significantly different for the unstabilized and stabilized materials, the resilient modulus did not increase significantly for the stabilized sections (Wayne et al. 2011b); in this study, geogrid was placed at the middle of the base layer in the stabilized sections, which were composed of a 12-in.-thick (305-mm-thick) base layer. One study performed on a dense-graded aggregate base layer focused on evaluating correlations between various geogrid index properties, such as junction and rib strength and pullout resistance. The results of plate load tests indicated that the change in stiffness achieved for a given aggregate base material depended on the properties of the geogrid (Hatami et al. 2012); in this study, geogrid was placed at one of three locations, including the base-subgrade interface, 1 in. (25 mm) above a geotextile that was placed at the base-subgrade interface, or directly on top of a geotextile that was placed at the base-subgrade interface in the stabilized sections, which each had an 8-in.-thick (203-mm-thick) base layer. In a different study, the results of plate load testing performed on laboratory-scale pavement sections with a crushed-stone aggregate base indicated that the same pavement life can be achieved with a base thickness that is reduced by up to 20 percent as a result of the inclusion of geogrid (Perkins 1999); in this study, geogrid was

placed at one of two locations, including the base-subgrade interface or the lower one-third position within the base layer in the stabilized sections, which each had a base layer that varied in thickness from 8 to 15 in. (203 to 381 mm) and an asphalt layer that was 3 in. (76 mm) thick. In a modified plate load test performed in a study specific to railway track structures, cyclic loading in a box was performed on ballast material. This research showed that there was an optimum geogrid aperture size for a given nominal aggregate size (Brown et al. 2007); in this study, geogrid was placed at one of two locations, including the ballast-subballast interface or 2 in. (51 mm) above the ballast-subballast interface in the stabilized sections, which each had a 12-in.-thick (305-mm-thick) base layer.

Triaxial shear testing involves compressive loading of a confined cylindrical test specimen at a constant vertical strain rate and measurement of the load sustained by the specimen during the testing as described in ASTM D7181 (Standard Test Method for Consolidated Drained Triaxial Compression Test for Soils). In one study, triaxial shear testing, which was performed at a rate of 10 percent strain per hour on crushed limestone specimen, showed that the strength and stiffness of geogrid-stabilized samples were higher than those of unstabilized samples and that greater improvement from geogrid was realized at higher strain levels (Nazzal et al. 2007); in this study, geogrid was placed at one of three locations, including the middle, upper one-third, or upper and lower one-third positions within the stabilized specimens, which were 6 in. (152 mm) in diameter and 12 in. (305 mm) in height.

RLT testing involves compressive loading of a confined cylindrical test specimen in repeated load pulses followed by rest periods as described in Appendix B of National Cooperative Highway Research Program (NCHRP) Report 598 (NCHRP 2004b) or AASHTO T 307. Multiple studies using RLT testing to investigate the permanent deformation and resilient

modulus of geogrid-stabilized samples have found that geogrid stabilization reduced permanent deformation but did not significantly increase resilient modulus (Abu-Farsakh et al. 2012, Moghaddas-Nejad and Small 2003, Nazzal et al. 2007, Perkins et al. 2004, Wayne et al. 2011b); in these studies, "common" crushed aggregate, crushed limestone aggregate, finely crushed basaltic aggregate, and RAP with RCA were evaluated with geogrid placed at the middle, lower one-third, upper one-third, and/or upper and lower one-third positions within the stabilized specimens, which were either 6 in. (152 mm) in diameter and 12 in. (305 mm) in height, 9 in. (229 mm) in diameter and 18 in. (457 mm) in height, or 12 in. (305 mm) in diameter and 24 in. (610 mm) in height. However, another study that used RLT testing to evaluate RAP, RCA, and crushed brick indicated that the permanent deformation not only decreased by up to 37 percent but that the resilient modulus also increased by up to 55 percent for geogrid-stabilized specimens compared to unstabilized specimens (Rahman et al. 2014); in this study, geogrid was positioned at the middle of the stabilized specimens, which were 4 in. (102 mm) in diameter and 8 in. (203 mm) in height. Another study reported that specimens with a higher density above the geogrid, simulating the higher density possible because of the stabilizing effects of geogrid, exhibited a significant increase in resilient modulus when compared to unstabilized specimens (Wayne et al. 2011a); in this study, geogrid was placed at the middle of the stabilized specimens, which were 6 in. (152 mm) in diameter and 12 in. (305 mm) in height. In another study, RLT testing performed on crushed amphibolite showed that geogrid confines a region that extends approximately one specimen diameter above and below the geogrid (Perkins et al. 2004); in this study, geogrid was placed at the middle of the stabilized specimens, which were 12 in. (305 mm) in diameter and 24 in. (610 mm) in height. Another laboratory study utilized RLT testing to investigate the effect of varying geogrid position, geometry, and tensile properties on the structural capacity of aggregate

base materials and found that the location of the geogrid within the test specimens contributed most to the reduction in permanent strain in the specimens and that placing the geogrid at the upper one-third position within the specimen yielded better results than placing the geogrid at the middle of the specimen (Abu-Farsakh et al. 2012); in this study, geogrid was placed at one of three locations, including the middle, upper one-third, or upper and lower one-third positions within the stabilized specimens, which were 6 in. (152 mm) in diameter and 12 in. (305 mm) in height. Other studies have also concluded that varying the location of geogrid within specimens or laboratory-scale pavement sections can have a significant effect on test results (Chen and Abu-Farsakh 2012, Nazzal et al. 2007); nonetheless, as demonstrated in most of the cited studies, placing the geogrid at the middle is most common.

2.4.2 Field Testing

Numerous field experiments have been performed to better understand geogrid stabilization of aggregate base material. The experiments involved evaluation of pavement responses and properties, including cracking, rutting, and stiffness as measured in distress surveys and dynamic cone penetrometer (DCP) tests.

Distress surveys involve assessing the distresses, including cracking and rutting, evident in a pavement section. Distress surveys are commonly performed after accelerated pavement testing and full-scale field testing to evaluate pavement performance. Full-scale field testing involves constructing pavement sections and subjecting them to trafficking, usually in a controlled environment, and accelerated pavement testing involves subjecting pavement sections to specified levels of trafficking in a comparatively short period of time, usually using a testing assembly. A study performed using full-scale accelerated pavement testing with measurements

of rutting and cracking showed that placing the geogrid at the base-subgrade interface was best for thin aggregate base layers, while placing the geogrid within the base layer was best for thicker base layers (Al-Qadi et al. 2008); in this study, geogrid was placed at one of two locations, including the base-subgrade interface or the upper one-third position within the base layer in the stabilized sections, which each had a base layer that varied in thickness from 8 to 18 in. (203 to 457 mm). Another study performed using accelerated pavement testing on a one-third-scale model pavement section found that the resilient modulus of the pavement section was not significantly influenced by the inclusion of geogrid reinforcement, but rutting in the subgrade layer was reduced (Tang et al. 2013); in this study, geogrid was placed at the base-subgrade interface in the stabilized sections, which each had a 4-in.-thick (102-mm-thick) base layer and a 1.5-in.-thick (38-mm-thick) asphalt layer. In one study, researchers constructed a single-lane test track with different types of geogrid in many test sections with base thickness varying from 12 to 20 in. (305 to 508 mm) throughout the track; they found that 12-in.-thick (305-mm-thick) geogrid-stabilized base layers sustained the same amount of rutting as 20-in.-thick (508-mm-thick) unstabilized base layers (Cancelli and Montanelli 1999); in this study, geogrid was placed at the base-subgrade interface in the stabilized sections, which each had a base layer that varied in thickness from 12 to 20 in. (305 to 508 mm) and a 3-in.-thick (76-mm-thick) asphalt layer.

DCP testing involves recording the number of hammer drops required to drive a cone-tipped rod into the ground, and the penetration rate of the rod is used to estimate the in-situ strength of soils as described in ASTM D6951 (Standard Test Method for Use of the Dynamic Cone Penetrometer in Shallow Pavement Applications). In one study, DCP test results showed that a region of increased stiffness immediately above the geogrid layer was attained because of the lateral confinement provided by the geogrid (Kwon et al. 2008); in this study, geogrid was

placed at one of two locations, including the base-subgrade interface or the lower one-third position within the base layer in the stabilized section, which had a base layer that varied in thickness from 8 to 18 in. (203 to 457 mm) and an asphalt layer that was 3 in. (76 mm) thick. In another study, the results of DCP tests performed on unstabilized and geogrid-stabilized pavement sections after 5 years of trafficking showed that the stabilized base materials had a region extending 4 to 6 in. (102 to 152 mm) above the geogrid with increased stiffness when compared to the unstabilized materials (Kwon and Tutumluer 2009); in this study, geogrid was placed at the base-subgrade interface in the stabilized sections, which each had a base layer that varied in thickness from 6 to 11 in. (152 to 279 mm) and an asphalt layer that was 9 to 11 in. (229 to 279 mm) thick.

2.5 Summary

Flexible pavements are generally designed to have multiple layers of varying mechanical properties, with stronger layers placed over weaker layers. The layers normally included in flexible pavement are a surface course composed of hot mix asphalt, a base course composed of aggregate base material, and the natural soil that exists on site, known as the subgrade. Each layer protects the layers beneath by decreasing the magnitude of traffic-induced stresses that are transferred downwards into the pavement structure. The interparticle friction in the base course, especially between the larger aggregates, allows the base layer to spread traffic loads over the subgrade. Weak subgrade materials can cause difficulty in road construction because they may not offer sufficient support for compaction of overlying base materials to an appropriate density. In order to improve the construction platform, geogrid is sometimes placed over weak subgrades, which can lead to better compaction and greater strength of the base material.

Many laboratory and field studies regarding geogrid stabilization and pavement performance have been conducted to investigate the benefits of geogrid-stabilized aggregate base materials in flexible pavements. Laboratory testing has involved evaluation of a number of material properties as measured in the plate load test, triaxial shear test, and RLT test. Field testing has involved evaluation of pavement responses and properties as measured in distress surveys and DCP tests. Multiple laboratory studies have shown increases in modulus as a result of geogrid stabilization, while other studies have not shown increases. Likewise, some field studies have shown increases in modulus and stiffness as a result of geogrid stabilization, while other studies have not shown increases. Variations in testing protocols, specimen dimensions, materials, and geogrid placement may all contribute to the inconsistent results of these laboratory and field studies on geogrid stabilization of aggregate base materials.

3 PROCEDURES

3.1 Overview

This research was motivated by the need to compare the results of laboratory quick shear testing on unstabilized and geogrid-stabilized aggregate base specimens with corresponding measurements of structural capacity of aggregate base materials obtained in the field. While this research does not directly compare the results of laboratory and field testing, it provides laboratory test results for aggregate base materials and geogrid products that are also the subject of ongoing full-scale field testing. In this research, laboratory specimens were prepared using the same aggregate base materials and geogrid products used at sites in northern Utah where corresponding full-scale field testing programs have been established. A future analysis will compare the results of this laboratory testing with the results of the ongoing field testing. This chapter describes the experimental design, materials characterization, test procedures, and statistical analyses performed for this research.

3.2 Experimental Design

The experimental design for this research is presented in Table 3-1. Testing was performed on aggregate base materials from three different sites where full-scale field testing programs have been established. All three sites are located in northern Utah, with two of the research sites being located in Utah County and one in Duschene County, hereafter referred to as

Table 3-1: Experimental Design

Material	Geogrid Product	Geogrid Configuration
Orem	None	-
	A	Single Layer
	B	Single Layer
	C	Single Layer
	D	Single Layer
	E	Single Layer
Springville	None	-
	A	Single Layer
	B	Single Layer
	C	Single Layer
	D	Single Layer
	E	Single Layer
Wells Draw Road	None	-
	B	Single Layer
	B	Double Layer

Orem, Springville, and Wells Draw Road, respectively. The base materials collected from each of the three research sites are representative of aggregate base materials commonly used on Utah Department of Transportation projects and also exhibit different particle angularity; as depicted in Figures 3-1, 3-2, and 3-3, the Orem base material is a crushed slag, the Springville material is an angular, crushed gravel, and the Wells Draw Road material is predominantly a rounded gravel.

In addition to testing of unstabilized control specimens, testing was also performed on specimens stabilized with one of five different geogrid types, each categorized as either BX or TX. Use of these different geogrid types ensured that the experimentation was both representative of the geogrid products available in the industry at the time of the study and consistent with the experimental designs employed at the field sites. Four biaxial geogrids and

Figure 3-1: Orem aggregate base material.

Figure 3-2: Springville aggregate base material.

Figure 3-3: Wells Draw Road aggregate base material.

one triaxial geogrid, shown in Figure 3-4 and hereafter referred to as geogrids A, B, C, D, and E, respectively, were used in this research.

The geogrid configurations that were tested for each combination of aggregate and geogrid were the same as those utilized in the field. In the case of the material from the sites in Orem and Springville, a single layer of geogrid placed at an upper one-third position within the specimen was tested. By contrast, the material from Wells Draw Road was tested in configurations with both single and double layers of geogrid as shown in Figure 3-5. Consistent with the results of previous research (Abu-Farsakh et al. 2012), the single-layer configuration involved placement of geogrid at the upper one-third position within the specimens, while the double-layer configuration involved placement of geogrid at the upper and lower one-third positions within the specimens. Two replicates of each configuration were tested to allow for statistical analyses of the results.

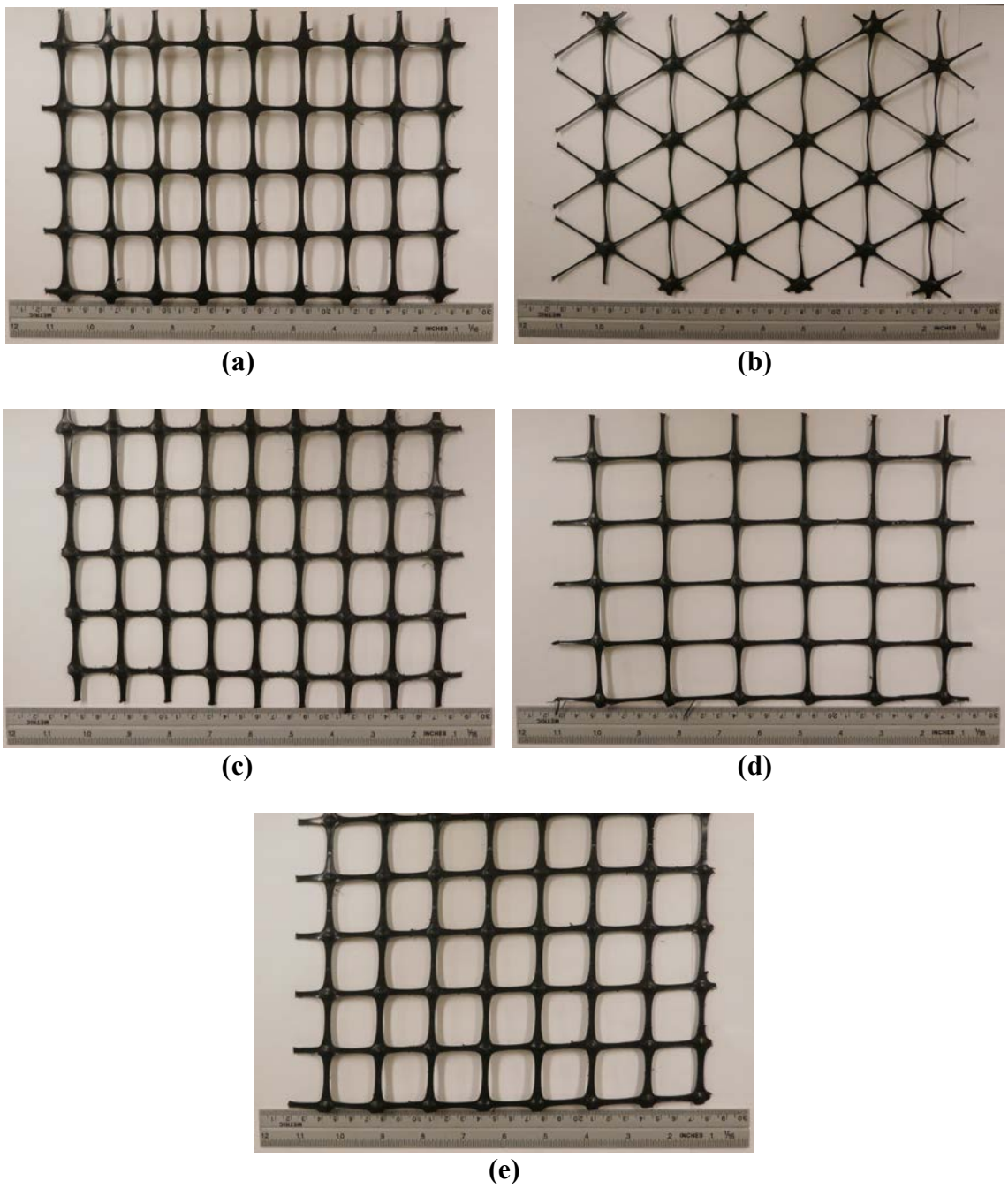

Figure 3-4: Geogrid products used in this research: (a) A, (b) B, (c) C, (d) D, and (e) E.

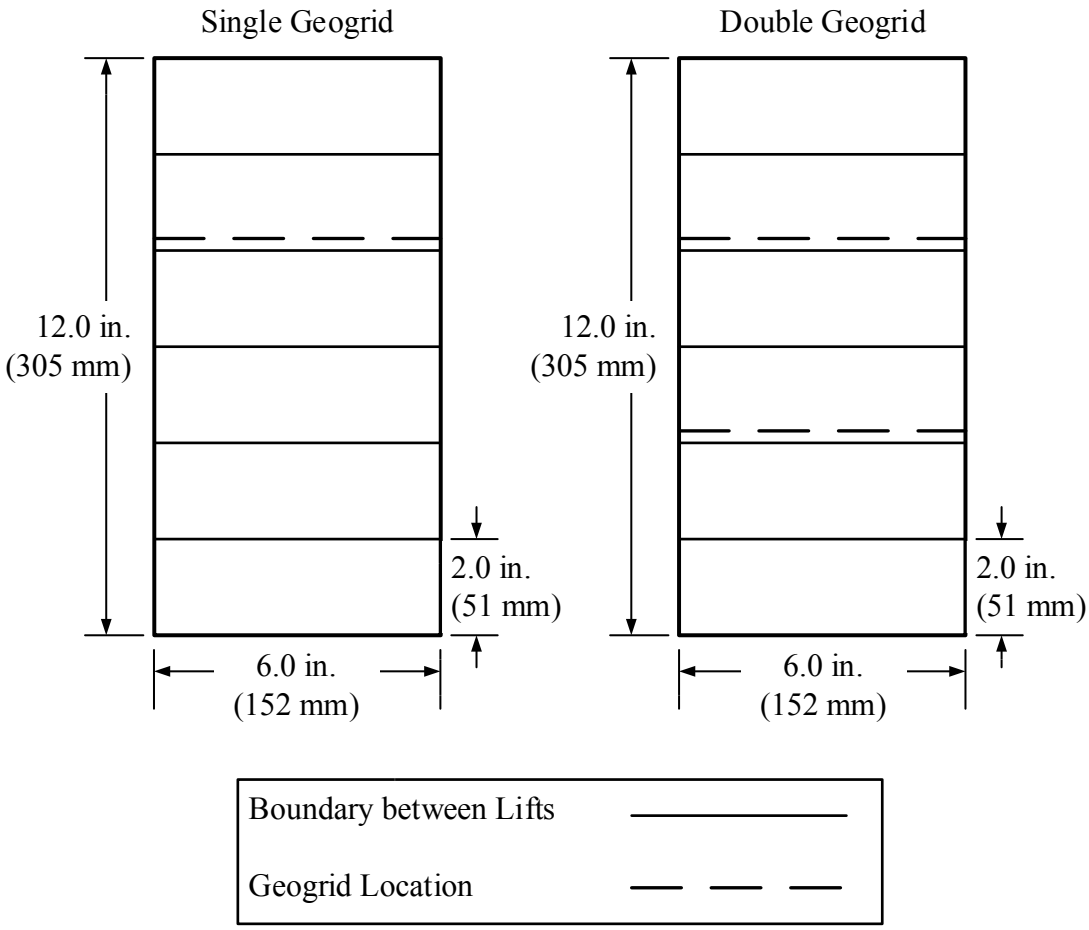

Figure 3-5: Testing configuration for quick shear testing.

The compaction procedure was the same for each specimen, regardless of the stabilization configuration. In configurations with one layer of geogrid, the geogrid was placed on top of the fourth of six lifts. In configurations with two layers of geogrid, the first geogrid was placed on top of the second of six lifts, and a second layer was placed on top of the fourth of six lifts. In all configurations, even though the surface of each intermediate lift was lightly scarified after compaction, the interlock between the aggregate and the geogrid resulted mainly from top-down penetration of the aggregate into the geogrid apertures.

3.3 Materials Characterization

Important material properties, including the particle-size distribution, soil classification, and moisture-density relationship were determined for each of the sampled aggregate base materials. The following sections outline the laboratory procedures associated with this testing.

3.3.1 Particle-Size Distribution and Soil Classification

The particle-size distribution of the soil was determined in general accordance with ASTM D6913 (Standard Test Methods for Particle-Size Distribution (Gradation) of Soils Using Sieve Analysis). Upon delivery to the laboratory, each aggregate base material sample was dried in an oven at 140°F (60°C) for at least 24 hours. Each material was then separated across the 3/4 in. (19 mm), 1/2 in. (13 mm), 3/8 in. (9.5 mm), No. 4 (4.8 mm), No. 8 (2.4 mm), No. 16 (1.2 mm), No. 30 (0.60 mm), No. 50 (0.30 mm), No. 100 (0.15 mm), and No. 200 (0.074 mm) sieve sizes. The materials retained on each sieve were then placed in different containers for storage. The total weight of each material retained on each sieve was recorded, and the percent by dry weight of material retained on each sieve size was then calculated as a basis for preparing samples with the same particle-size distributions for further testing.

A washed sieve analysis was then performed in general accordance with ASTM C136 (Standard Test Method for Sieve Analysis of Fine and Coarse Aggregates). For each aggregate, a 3-lb (1361-g) sample was prepared following the previously prepared particle-size distribution. Each sample was washed over the same set of sieves used in the earlier sieve analysis, and the material retained on each sieve size was dried in the oven at 140°F (60°C) for at least 24 hours until reaching constant weight. The material was then weighed, and the percent by dry weight of material retained on each sieve size was then calculated as the basis for classifying each material.

The plasticity index (PI) for each material was determined in general accordance with ASTM D4318 (Standard Test Methods for Liquid Limit, Plastic Limit, and Plasticity Index of Soils). A representative 1-lb (454-g) sample of each material passing the No. 40 (0.42 mm) sieve was prepared for this testing. If a plastic limit could not be determined, then the material was determined to be non-plastic. If the material was plastic, the liquid limit test was also performed. For materials for which a plastic limit could be determined, the PI was determined as the difference between the plastic limit and the liquid limit. Once the washed particle-size distributions and PIs were measured, the AASHTO and Unified soil classifications were determined in general accordance with AASHTO M 145 (Classification of Soils and Soil-Aggregate Mixtures for Highway Construction Purposes) and ASTM D2487 (Standard Practice for Classification of Soils for Engineering Purposes (Unified Soil Classification System)), respectively.

3.3.2 Moisture-Density Relationship

The optimum moisture content (OMC) and maximum dry density (MDD) were determined from the moisture-density relationship for each aggregate base material in general accordance with ASTM D1557 (Standard Test Methods for Laboratory Compaction Characteristics of Soil Using Modified Effort (56,000 ft-lbf/ft^3 (2,700 kN-m/m^3))). Four or five specimens of each material were prepared for this testing. In each case, the amounts of each sieve size necessary to produce a specimen 6.0 in. (152 mm) in diameter and 4.6 in. (117 mm) in height were weighed out according to the results of the sieve analysis performed on the bulk material. The aggregates were then oven-dried at 140°F (60°C) for at least 24 hours to remove any residual moisture that may have accumulated in the material during storage. After being

removed from the oven and allowed to cool to room temperature, the dried aggregates were then moistened at target gravimetric moisture contents ranging between 3.0 and 11.0 percent by weight of dry aggregate.

The specimens were then compacted into a steel mold with 56 blows of a 10-lb (4536-g) hammer dropped from a height of 18 in. (457 mm) applied to each of five lifts per specimen. The specimen surface was scarified between lifts, and, to flatten the top surface of the specimen, three drops of a 10-lb (4536-g) finishing tool were applied from a height of 18 in. (457 mm) onto a 6-in. (152-mm)-diameter plate placed on top of the compacted specimen. The weights and heights of the specimens were measured after compaction, and the specimens were then extruded and oven-dried at 140°F (60°C) for at least 48 hours or until constant weight. The resulting dry weights of the specimens were used together with the previously measured weights and heights to compute the moisture content and dry density of each specimen. For each aggregate, the dry density measurements were then plotted against the corresponding moisture content measurements, an approximately parabolic curve was fit to the data, and the OMC and MDD were estimated graphically.

3.4 Quick Shear Testing

As previously discussed, geogrid-stabilized and unstabilized control specimens were evaluated using the AASHTO T 307 quick shear testing protocol. The computer-controlled, servo-hydraulic UTM-100 equipment available in the Brigham Young University Highway Materials Laboratory was utilized for the testing. Figure 3-6 displays the UTM-100 setup in the laboratory. The specimen preparation and testing procedures are outlined in this section.

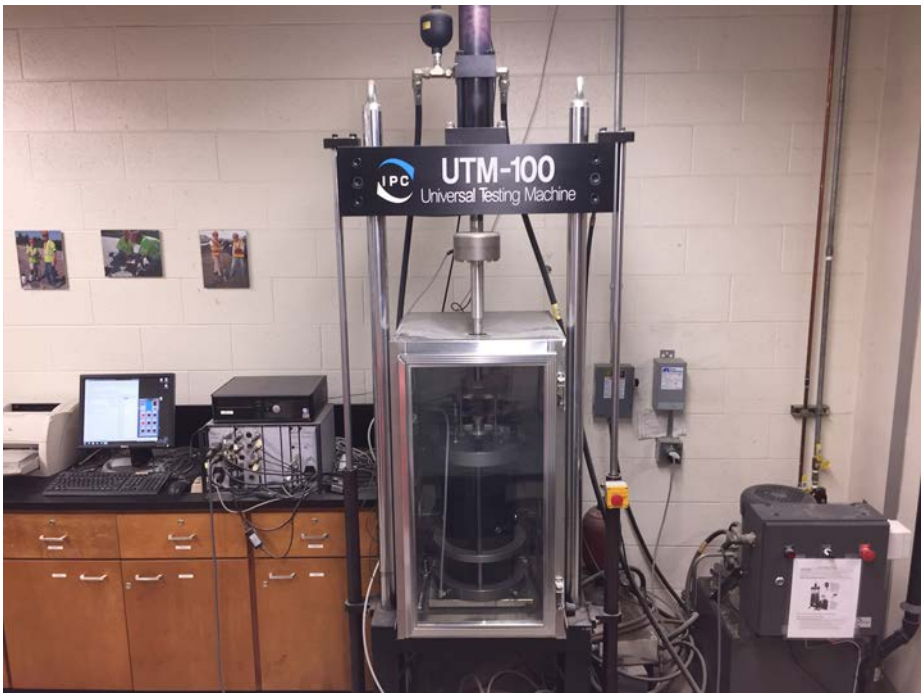

Figure 3-6: UTM-100 testing equipment.

The test specimens were prepared using representative amounts of each sieve size as determined from the particle-size distribution analyses performed earlier. After being weighed out, the aggregate samples were placed in an oven at 140°F (60°C) for at least 24 hours to remove any residual moisture. The samples were then removed from the oven and allowed to cool to room temperature. Once the samples were cooled, an appropriate amount of water was added to bring the gravimetric water content of the specimens to slightly above the previously determined OMC; an additional 0.3 to 0.5 percent of water was added to each specimen to compensate for the amount of water evaporation typically observed to occur during the remaining procedures.. The water was mixed into the aggregate samples until uniform color and texture were achieved. The moistened aggregates were then sealed in an airtight plastic bag and allowed to equilibrate for 24 hours.

The specimens were compacted in a custom-made split steel mold with an inner diameter of 6 in. (152 mm) and a height of 12 in. (305 mm), which was fastened to a steel base plate as shown in Figure 3-7. The mold was prepared by first placing two layers each of aluminum foil and paper towel on the base plate to provide support to the bottom of the compacted specimen when it was later transferred from the base plate. A latex membrane was placed inside the mold. The mold was secured to the base plate, and a collar was placed on top of the mold to prevent damage to the top of the inner membrane during the compaction process. Specimens were compacted manually in lifts of approximately equal weight in general accordance with ASTM

Figure 3-7: Steel split mold for compacting specimens.

D1557. To achieve a modified Proctor compaction effort of 56,000 ft-lbf/ft^3 (2,700 kN-m/m^3), specimens were constructed in six 2-in. (51-mm)-thick lifts with 122 blows per lift applied using a 10-lb (4.5-kg) hammer dropped from a height of 18 in. (457 mm). Prior to placement of another lift in the mold, a flathead screwdriver was used to lightly scarify the surface of each compacted lift to a depth of about 0.125 in. (3 mm) in three parallel lines, which were 1.5 to 2.0 in. (38 to 51 mm) apart, and another three similarly spaced parallel lines perpendicular to the first three. Care was taken not to dislodge large aggregates during this process. Geogrid circles having a diameter of approximately 5.8 in. (147 mm), as shown in the examples of geogrid type in Figure 1-1, were cut from geogrid rolls supplied by the respective manufacturers and placed within the specimens at either the upper one-third or upper and lower one-third position depending on the geogrid configuration. The geogrid circles were cut in such a way as to preserve the maximum number of intact apertures. Upon completion of the final lift, a finishing tool was used to flatten the top of the specimens; in this process, three drops of a 10-lb (4.5-kg) hammer were applied from a height of 18 in. (457 mm) onto a 6-in. (152-mm)-diameter plate placed on top of the compacted specimen.

After compaction of a specimen was complete, the specimen and mold were removed from the base plate and placed on top of a saturated, 2-in. (51-mm)-thick, 6-in. (152-mm)-diameter porous stone. The mold was then removed from around the specimen, and another saturated porous stone was placed on top of the specimen. A second membrane was placed around the specimen using a membrane expander as shown in Figure 3-8, and the specimen and porous stones were sealed in an airtight plastic bag and left to equilibrate at room temperature for 16 to 24 hours.

Figure 3-8: Membrane expander.

When a specimen was ready for placement in the triaxial cell, a saturated, 0.5-in. (13-mm) thick, 6-in. (152-mm)-diameter porous bronze disk was placed on top of the 6-in. (152-mm)-diameter lower metal platen within the triaxial cell. The upper porous stone was removed from the specimen, and the specimen was then moved off the lower porous stone and placed on top of the porous disk. Another 6-in. (152 mm)-diameter metal platen was placed on top of the specimen, and rubber O-rings were used to create an airtight seal between the metal platens and membranes. The top of the triaxial cell was then bolted in place over the specimen, and the entire apparatus was placed into the UTM-100 as shown in Figure 3-9. During testing, a pressure

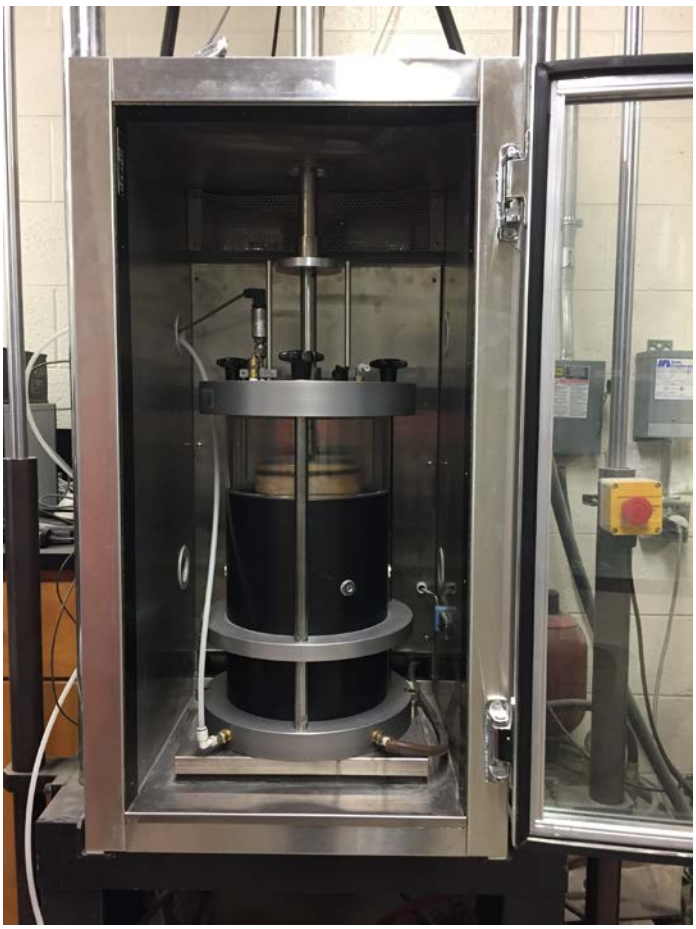

Figure 3-9: Triaxial cell placed inside the UTM-100.

transducer was used to measure the air pressure inside the triaxial cell, and a hole in the center of the lower platen allowed water to drain freely from the specimen.

Quick shear testing was performed in general accordance with the applicable portions of AASHTO T 307. Because the focus of this study was on shear testing, the specimens were subjected only to the shear portion of the test; the conditioning and resilient modulus portions of the test were not performed. The testing consisted of measuring the compressive load while subjecting the specimens to a constant strain rate of 0.12 in. (3 mm) per minute, which corresponds to 1 percent strain per minute. The confining pressure remained constant at 5 psi (35 kPa) throughout the testing.

The specimens were allowed to equilibrate for several minutes until reaching constant height under the applied confining pressure before the testing commenced. Measurements of load and axial displacement were recorded and used to develop a stress-strain plot for each specimen tested. The test stopped when the specimens reached 15 percent strain, and the peak axial stress was recorded. The modulus to the peak axial stress, the modulus of the elastic portion of the curve, and the modulus at 2 percent strain were then calculated.

The modulus to the peak axial stress was calculated by dividing the peak stress by the corresponding strain. The modulus of the elastic portion of the curve was calculated as the slope of a linear trend line computed for a middle portion of the stress-strain curve between the start of the test and the greater of the peak stress or the stress corresponding to a level of 10 percent strain; specifically, the curve in this range was divided into four segments of equal length, and the slope of the second segment was analyzed. A maximum strain value of 10 percent was chosen in this analysis because all of the specimens experienced plastic deformation at this strain level. The modulus at 2 percent strain was calculated by dividing the stress corresponding to 2 percent strain by a strain value of 2 percent. Linear interpolation was used when necessary to determine the exact value of stress corresponding to 2 percent strain in each test.

After the testing, the specimens were dried to constant weight, and the gravimetric moisture content was calculated. The dry density of each specimen was estimated from the wet density measured immediately after compaction and the moisture content measured immediately after testing. Preparation and testing of a specimen were repeated if the coefficient of variation computed for any of the results obtained from a given set of two replicates was greater than 25 percent.

3.5 Statistical Analyses

Two analyses of variance (ANOVAs) were performed on each result of the laboratory testing for each of the three aggregate base materials included in this research. One ANOVA was performed to investigate differences between geogrid-stabilized specimens and unstabilized control specimens, without distinguishing among geogrid products or geogrid configurations, while the other was performed to investigate differences between individual geogrid products or geogrid configurations. (The intent of the second analysis was not to suggest that a given geogrid product is generally better than another but rather to investigate the differences in compatibility of the different geogrid products with the specific aggregate base materials included in this research.) In the first ANOVA, the independent variable was condition, where a specimen was either stabilized or unstabilized. In the second ANOVA, the independent variable was geogrid product or geogrid configuration, where a specimen was stabilized with a particular geogrid product in a particular geogrid configuration or unstabilized. In both ANOVAs, the potential covariates were moisture content, as measured immediately after testing, and dry density, and the dependent variables were the peak axial stress, modulus to the peak stress, elastic modulus, and modulus at 2 percent strain. In each ANOVA model, when either of the two covariates had a *p*-value greater than 0.05, it was removed one at a time from the model, which was then run again; the final model included only covariates with *p*-values less than or equal to 0.05. The least squares means for the independent variable, adjusted for the included covariates, were then computed. In addition, for the second ANOVA, Tukey's method was utilized to compare the individual geogrid products or geogrid configurations. When a *p*-value less than or equal to 0.05 was computed for a given comparison, the difference between the products or configurations was determined to be statistically significant.

3.6 Summary

This research was motivated by the need to compare the results of laboratory quick shear testing on unstabilized and geogrid-stabilized aggregate base specimens with corresponding measurements of structural capacity of aggregate base materials obtained in the field. While this research does not directly compare the results of laboratory and field testing, it provides laboratory test results for aggregate base materials and geogrid products that are also the subject of ongoing full-scale field testing. A future analysis will compare the results of this laboratory testing with the results of the ongoing field testing. In addition to testing of unstabilized control specimens, testing was also performed on specimens stabilized with one of five different geogrid types, each categorized as either BX or TX. Two replicates of each configuration were tested to allow for statistical analyses of the results. Important material properties, including the particle-size distribution, soil classification, and moisture-density relationship were determined for each of the sampled aggregate base materials.

Geogrid-stabilized and unstabilized control specimens were evaluated using the AASHTO T 307 quick shear testing protocol. Measurements of load and axial displacement were recorded and used to develop a stress-strain plot for each specimen tested. The peak axial stress, the modulus to the peak axial stress, the modulus of the elastic portion of the curve, and the modulus at 2 percent strain were then calculated. After the testing, the gravimetric moisture content and dry density of each specimen were calculated. Statistical analyses were then performed to investigate differences between geogrid-stabilized specimens and unstabilized control specimens and to investigate differences between individual geogrid products or geogrid configurations. (The intent of the analysis was not to suggest that a given geogrid product is

generally better than another but rather to investigate the differences in compatibility of the different geogrid products with the specific aggregate base materials included in this research.)

4 RESULTS AND ANALYSIS

4.1 Overview

This chapter presents the results of both the laboratory testing and the statistical analyses performed for this research. As explained in Chapter 3, the aggregate base materials and geogrid types were selected to ensure that the experimental design for this research matched that of the ongoing full-scale field testing. All results from this research are limited in their application to the aggregate base material types, geogrid products, and geogrid configurations associated with this study.

4.2 Materials Characterization

Materials characterization included washed sieve analysis, Atterberg limits testing, soil classification, and determination of OMC and MDD for each aggregate base material. The following sections present the results of the materials characterization.

4.2.1 Particle-Size Distribution and Soil Classification

The results of the washed sieve analyses are plotted in Figure 4-1, which shows that the Orem and Springville materials are coarser than the Wells Draw Road material. Atterberg limits testing indicated that the base materials from the Orem and Springville sites were non-plastic and that the Wells Draw Road material was slightly plastic, having a PI of 1.5. Based on the washed

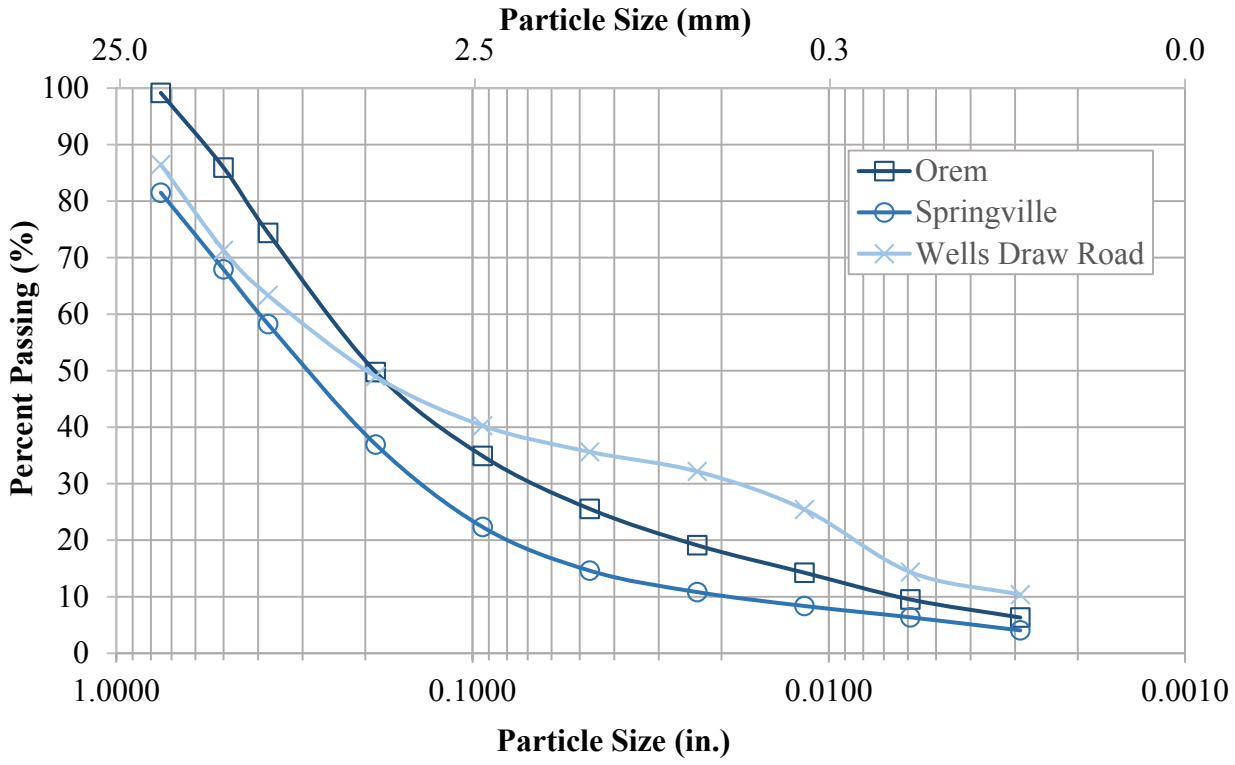

Figure 4-1: Particle-size distribution.

sieve analyses and the Atterberg limits testing, the Orem material was classified as A-1-a and GW-GM (well-graded gravel with silt and sand), the Springville material was classified as A-1-a and GW (well-graded gravel with sand), and the Wells Draw Road material was classified as A-1-a and GP-GM (poorly-graded gravel with silt and sand) according to the AASHTO and USCS methods, respectively.

Regarding the base materials, the D_{50} and D_{85} values ranged from 0.2 to 0.3 in. (5 to 8 mm) and from 0.5 to 0.8 in. (13 to 20 mm), respectively. Therefore, based on Federal Highway Administration recommendations (FHWA 2008), the minimum geogrid aperture size for the three base materials was 0.5 in. (13 mm), and the maximum geogrid apertures sizes ranged from 1.0 to 1.6 in. (25 to 41 mm), respectively. Table 4-1 depicts each of the three base materials with

Table 4-1: Recommended Minimum and Maximum Aperture Sizes

Material	Aggregate Property		Recommended Geogrid Aperture Size	
	D_{50}, in. (mm)	D_{85}, in. (mm)	Minimum, in. (mm)	Maximum, in. (mm)
Orem	0.2 (5)	0.5 (13)	0.5 (13)	1.0 (25)
Springville	0.3 (8)	0.8 (20)	0.5 (13)	1.6 (41)
Wells Draw Road	0.2 (5)	0.75 (19)	0.5 (13)	1.5 (38)

their corresponding D_{50}, D_{85}, and maximum and minimum aperture size values. Among the geogrids selected for use in this research, all of the geogrid products except B and D met the recommendations for the Orem base material, and all of the geogrids met the recommendations for the Springville and Wells Draw Road base materials. Geogrid product B, in particular, was not available in a size that met the recommendations for the Orem base material, but, like geogrid product D, it is commonly used with similar base materials according to the manufacturer.

4.2.2 Moisture-Density Relationship

The OMC and MDD values obtained from moisture-density testing of the materials are presented in Table 4-2, and the corresponding moisture-density curves are presented in Appendix A.

Table 4-2: Moisture-Density Relationships

Material	Optimum Moisture Content (%)	Maximum Dry Density, lb/ft^3 (kg/m^3)
Orem	9.5	127.1 (2036)
Springville	4.9	128.4 (2057)
Wells Draw Road	5.5	137.2 (2198)

4.3 Quick Shear Testing

The average test results obtained from the quick shear tests are given in Table 4-3; two replicate specimens were evaluated in each test, and all of the coefficients of variation were less than 15 percent after selected tests were repeated. Data for individual specimens, including those that were omitted because the resulting coefficient of variation was greater than 25 percent, are provided in Appendix B, and post-testing photographs of each specimen are presented in Appendix C. Of the 27 total specimens that were tested with geogrid, failure of the geogrid occurred only twice, and both occurrences involved a rib failure in geogrid product B when it was placed in a double-layer configuration within the Wells Draw Road material; Figure 4-2 displays an example of the rib failure that was typical of both specimens. The results of statistical analyses and discussion of the data are provided in the next section.

4.4 Statistical Analyses

As explained in Chapter 3, two ANOVAs were performed on each result of the laboratory testing for each of the three aggregate base materials included in this research. For each aggregate base material, one ANOVA was performed to investigate differences between geogrid-stabilized specimens and unstabilized control specimens, without distinguishing among geogrid products or geogrid configurations, while the other was performed to investigate differences between individual geogrid products or geogrid configurations. (The intent of the second analysis was not to suggest that a given geogrid product is generally better than another but rather to investigate the differences in compatibility of the different geogrid products with the specific aggregate base materials included in this research.)

Table 4-3: Average Quick Shear Test Results

Material	Geogrid Product	Average Peak Axial Stress, psi (kPa)		Average Modulus to Peak Stress, psi (kPa)		Average Elastic Modulus, psi (kPa)		Average Modulus at 2% Strain, psi (kPa)	
Orem	None	133.1	(918)	520.2	(3586)	6154.1	(42431)	549.0	(3785)
	A	188.7	(1301)	516.8	(3563)	6126.5	(42241)	687.0	(4737)
	B	161.2	(1112)	436.8	(3012)	5193.5	(35808)	567.6	(3914)
	C	178.1	(1228)	490.4	(3381)	5838.1	(40252)	636.2	(4386)
	D	171.0	(1179)	481.0	(3317)	5676.2	(39136)	639.5	(4409)
	E	173.7	(1197)	440.7	(3039)	5304.3	(36572)	554.2	(3821)
Springville	None	72.7	(501)	350.0	(2413)	4133.7	(28501)	304.4	(2099)
	A	105.4	(727)	243.3	(1678)	2911.9	(20077)	345.2	(2380)
	B	92.5	(638)	249.8	(1722)	3016.0	(20795)	352.0	(2427)
	C	97.8	(675)	316.1	(2179)	3788.1	(26118)	387.7	(2673)
	D	89.1	(614)	271.2	(1870)	3265.3	(22513)	350.0	(2413)
	E	103.7	(715)	295.2	(2035)	3482.4	(24010)	392.1	(2703)
Wells Draw Road	None	77.0	(531)	181.4	(1251)	2158.6	(14883)	235.9	(1627)
	B (Single)	96.5	(665)	221.3	(1526)	2643.3	(18225)	279.1	(1925)
	B (Double)	98.5	(679)	151.0	(1041)	1813.6	(12504)	204.1	(1407)

Figure 4-2: Geogrid rib failure.

4.4.1 Effect of Geogrid Stabilization

The results of the ANOVAs performed to investigate differences between geogrid-stabilized specimens and unstabilized control specimens, without distinguishing among geogrid products or geogrid configurations, are presented in Tables 4-4 and 4-5 and Figures 4-3 through 4-6, with supporting data provided in Appendix D. In Table 4-4, *p*-values less than or equal to 0.05, which are presented in bold-face font, indicate a statistically significant difference between

Table 4-4: Statistical Analyses of Geogrid Condition

Material	*p* -values			
	Peak Axial Stress	Modulus to Peak Stress	Elastic Modulus	Modulus at 2% Strain
Orem	**0.000**	0.159	0.159	0.131
Springville	**0.001**	**0.027**	**0.038**	**0.024**
Wells Draw Road	**0.001**	0.889	0.863	0.886

Table 4-5: Least Squares Means and Corresponding Percent Change for Geogrid Condition

Material	Geogrid Condition	Peak Axial Stress, psi (kPa)		Percent Change (%)	Modulus to Peak Stress, psi (kPa)		Percent Change (%)	Elastic Modulus, psi (kPa)		Percent Change (%)	Modulus at 2% Strain, psi (kPa)		Percent Change (%)
Orem	Without	133.1	(918)		520.2	(3587)		6154	(42430)		549	(3785)	
	With	174.5	(1203)	31	473.1	(3262)	-	5628	(38804)	-	616.9	(4253)	-
Springville	Without	72.72	(501)		337.9	(2330)		3994	(27538)		304.4	(2099)	
	With	97.7	(674)	34	277.5	(1913)	-18	3321	(22897)	-17	365.4	(2519)	20
Wells Draw Road	Without	74.68	(515)		181.4	(1251)		2159	(14886)		235.9	(1626)	
	With	98.65	(680)	32	186.2	(1284)	-	2228	(15362)	-	241.6	(1666)	-

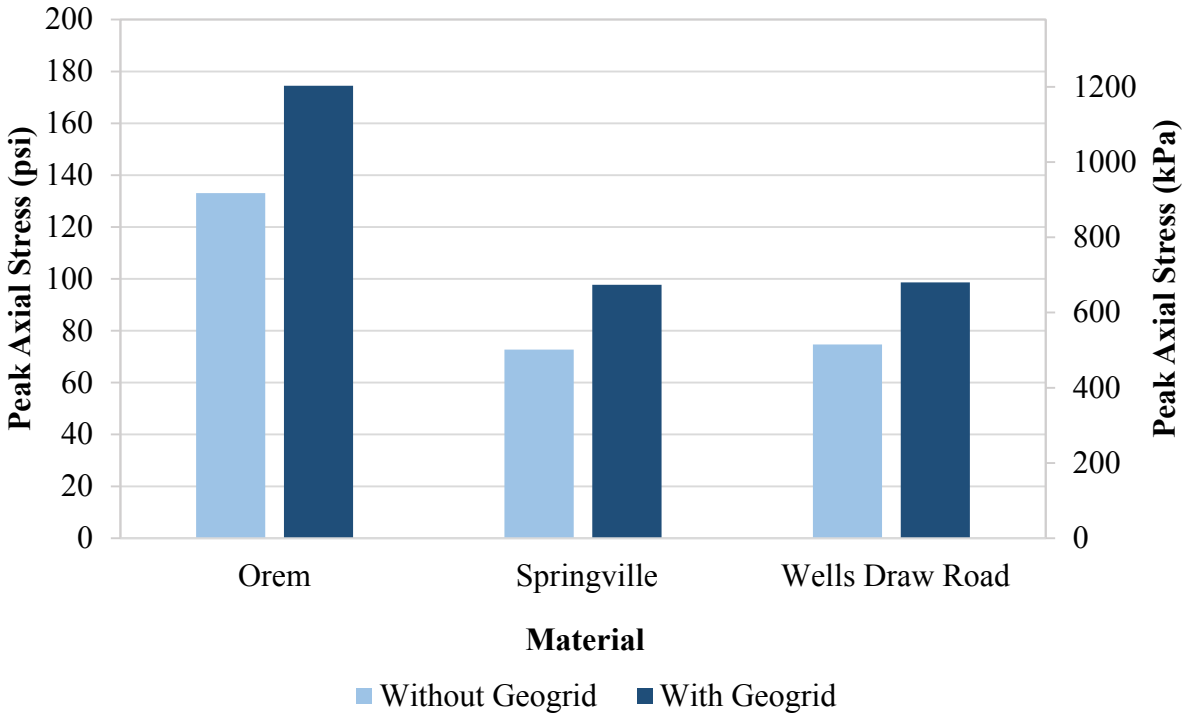

Figure 4-3: Least squares means for main effect on peak axial stress.

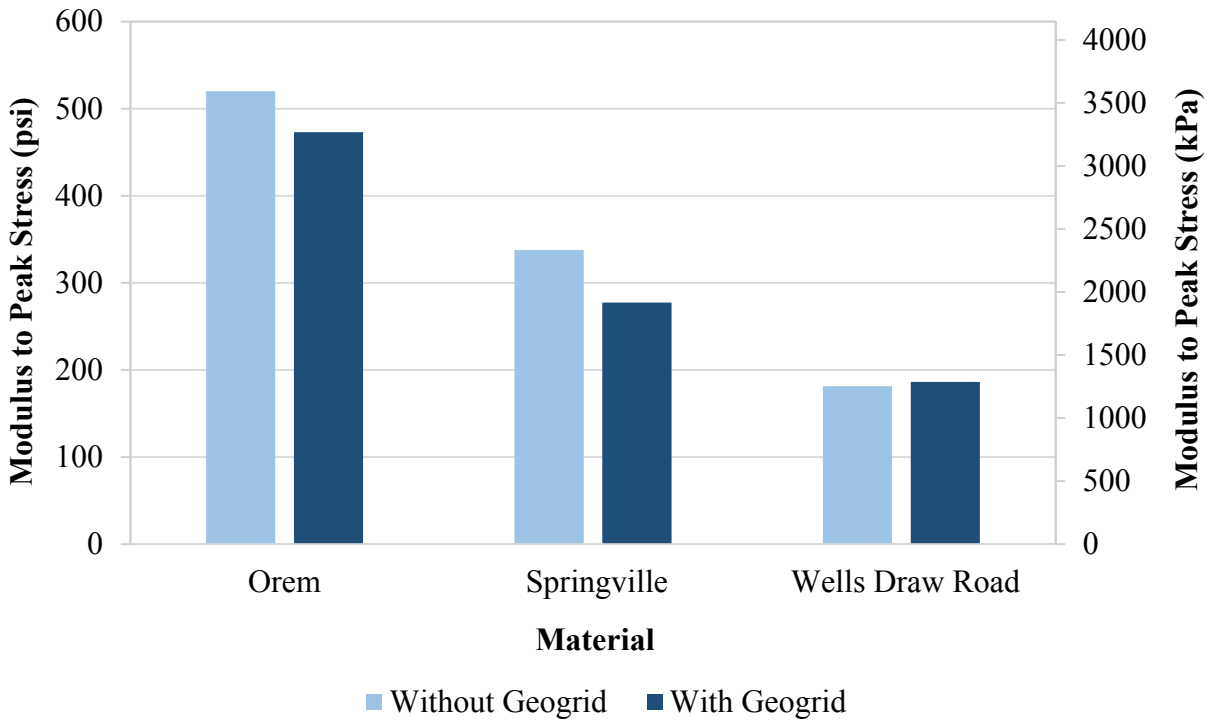

Figure 4-4: Least squares means for main effect on modulus to peak stress.

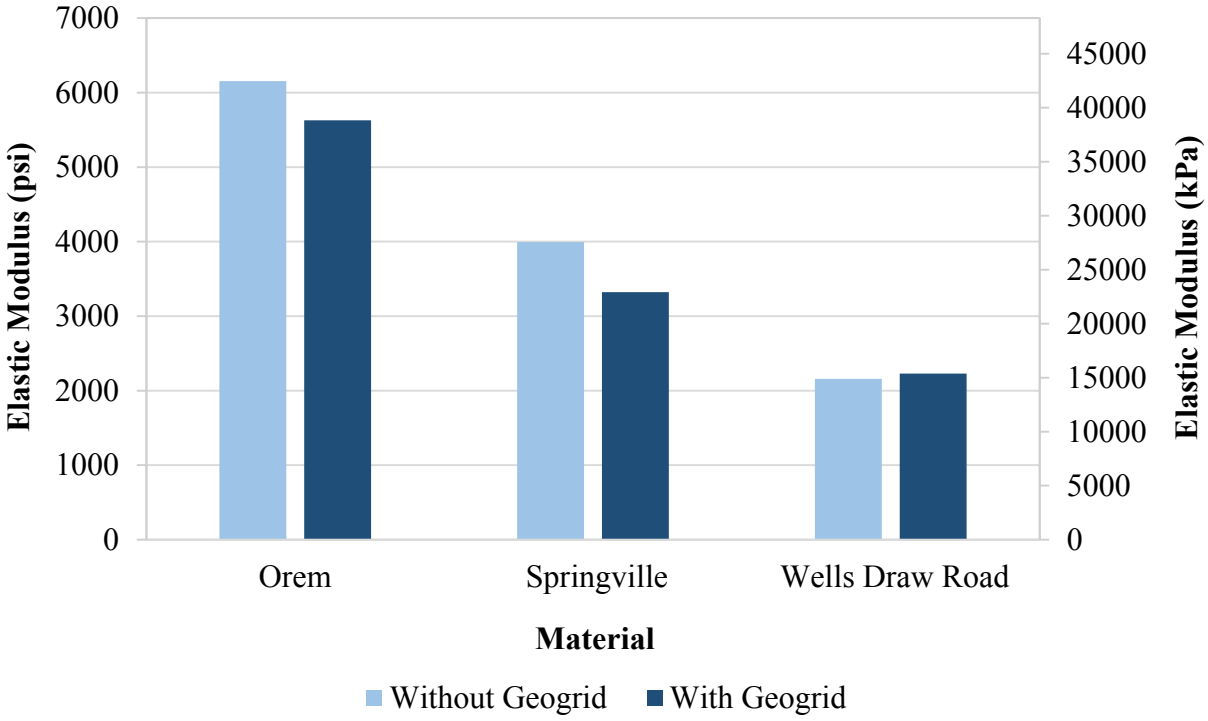

Figure 4-5: Least squares means for main effect on elastic modulus.

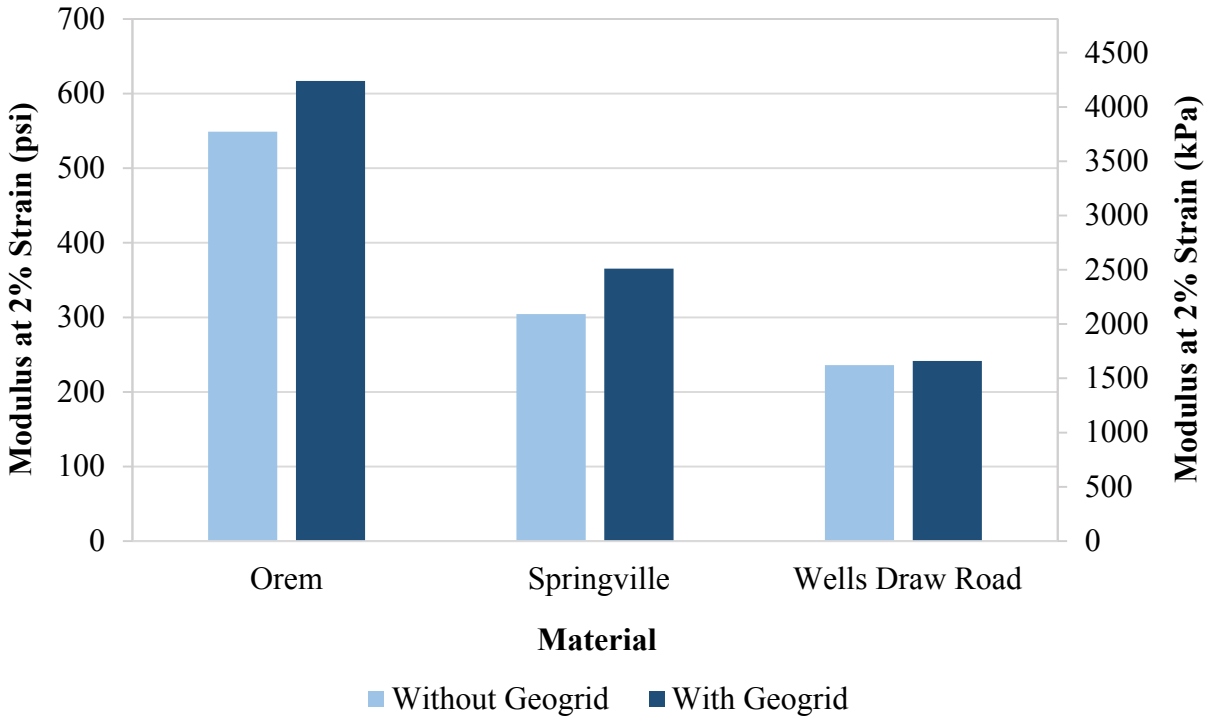

Figure 4-6: Least squares means for main effect on modulus at 2 percent strain.

the two levels of stabilization evaluated in this analysis (stabilized and unstabilized). The least squares means computed from each ANOVA model are presented in Table 4-5 with a corresponding percent change listed for the differences that are shown in Table 4-4 to be statistically significant. In Table 4-5, shading indicates the basis for the comparison (the unstabilized control specimens), and a hyphen indicates that the difference between the geogrid-stabilized specimens and the unstabilized control specimens was not statistically significant.

Regarding peak axial stress, statistically significant differences were observed for each of the three aggregate base materials. On average, geogrid stabilization increased the peak axial stress by 31, 34, and 32 percent for the Orem, Springville, and Wells Draw Road materials, respectively.

Regarding modulus to peak stress, a statistically significant difference between geogrid-stabilized specimens and unstabilized control specimens was observed for the Springville material, and the results indicate that geogrid stabilization decreased the modulus by 18 percent, on average. The difference in modulus to peak stress was not statistically significant for the Orem or Wells Draw Road material.

Regarding elastic modulus, a statistically significant decrease of 17 percent, on average, was observed for the Springville material. The difference in elastic modulus was not statistically significant for the Orem or Wells Draw Road material. Regarding modulus at 2 percent strain, a statistically significant increase of 20 percent, on average, was observed for the Springville material. The difference in modulus at 2 percent strain was not statistically significant for the Orem or Wells Draw Road material.

In summary, geogrid stabilization led to statistically significant increases of 31 to 34 percent in peak axial stress for all three materials, decreases of 17 to 18 percent in modulus to peak stress and elastic modulus for the Springville material, and an increase of 20 percent in modulus at 2 percent strain for the Springville material. Therefore, depending on the method of data analysis, the quick shear test results indicate that geogrid stabilization, with the effect of geogrid stabilization averaged across all of the geogrid products evaluated in this study, may or may not improve the structural quality of the aggregate base materials evaluated in this study. Among the modulus measurements, modulus at 2 percent strain was recommended in earlier laboratory research (Knighton 2015) due to its greater probability of consistently showing a benefit from geogrid stabilization for the two materials evaluated in that study; however, further research is needed to determine which method of data analysis yields the best comparisons with field test results.

4.4.2 *Effects of Geogrid Product and Configuration*

The results of the ANOVAs performed to investigate differences between individual geogrid products or geogrid configurations, are presented in Tables 4-6 and 4-7 and Figures 4-7 through 4-10, with supporting data provided in Appendix D. In Table 4-6, *p*-values less than or equal to 0.05, which are presented in bold-face font, indicate a statistically significant difference between at least two of the six levels of geogrid product (stabilized with geogrid products A, B, C, D, and E in a single-layer configuration or unstabilized for the Orem and Springville materials) or three levels of geogrid configuration (stabilized with geogrid product B in a single-layer or double-layer configuration or unstabilized for the Wells Draw Road material) evaluated in this analysis. The least squares means computed from each ANOVA model are presented in Table 4-7 with a corresponding percent change listed for the differences that are shown in Table 4-6 to be statistically significant. In Table 4-7, shading indicates the basis for the comparison (the unstabilized control specimens), and a hyphen indicates that the difference between the geogrid-stabilized specimens and the unstabilized control specimens was not statistically significant. For the results of Tukey's method, which are presented in Appendix D, *p*-values less than or equal to 0.05 indicate that the difference between two geogrid products or two geogrid configurations is statistically different. Although the results of Tukey's method include results

Table 4-6: Statistical Analyses of Geogrid Product

Material	*p* -values			
	Peak Axial Stress	Modulus to Peak Stress	Elastic Modulus	Modulus at 2% Strain
Orem	**0.000**	0.163	0.156	**0.009**
Springville	**0.005**	**0.050**	0.069	0.137
Wells Draw Road	**0.014**	**0.013**	**0.037**	0.119

Table 4-7: Least Squares Means and Corresponding Percent Improvement for Geogrid Product or Configuration

Material	Geogrid Product	Peak Axial Stress, psi (kPa)		Percent Change (%)	Modulus to Peak Stress, psi (kPa)		Percent Change (%)	Elastic Modulus, psi (kPa)		Percent Change (%)	Modulus at 2% Strain, psi (kPa)		Percent Change (%)
Orem	None	133.1	(918)		520.2	(3587)		6154	(42430)		549.0	(3785)	
	A	188.7	(1301)	42	516.8	(3563)	-	6126	(42237)	-	687.0	(4737)	25
	B	161.2	(1111)	21	436.8	(3012)	-	5194	(35811)	-	567.6	(3913)	-
	C	178.1	(1228)	34	490.4	(3381)	-	5838	(40252)	-	636.2	(4386)	-
	D	171.0	(1179)	28	481.0	(3316)	-	5676	(39135)	-	639.5	(4409)	-
	E	173.7	(1198)	31	440.7	(3039)	-	5304	(36570)	-	554.2	(3821)	-
Springville	None	72.7	(501)		350.0	(2413)		4143	(28565)		304.4	(2099)	
	A	105.4	(726)	45	243.3	(1677)	-	2912	(20078)	-	345.2	(2380)	-
	B	92.5	(638)	-	249.8	(1722)	-	3016	(20795)	-	352.0	(2427)	-
	C	97.8	(675)	35	316.1	(2179)	-	3788	(26117)	-	387.7	(2673)	-
	D	89.1	(614)	-	271.2	(1870)	-	3265	(22511)	-	350.0	(2413)	-
	E	103.7	(715)	43	295.2	(2035)	-	3482	(24008)	-	392.1	(2703)	-
Wells Draw Road	None	74.7	(515)		172.8	(1191)		2159	(14886)		235.9	(1626)	
	B (Single)	97.6	(673)	31	236.2	(1629)	37	2643	(18223)	-	279.1	(1924)	-
	B (Double)	99.7	(688)	34	144.7	(998)	-16	1814	(12507)	-	204.1	(1407)	-

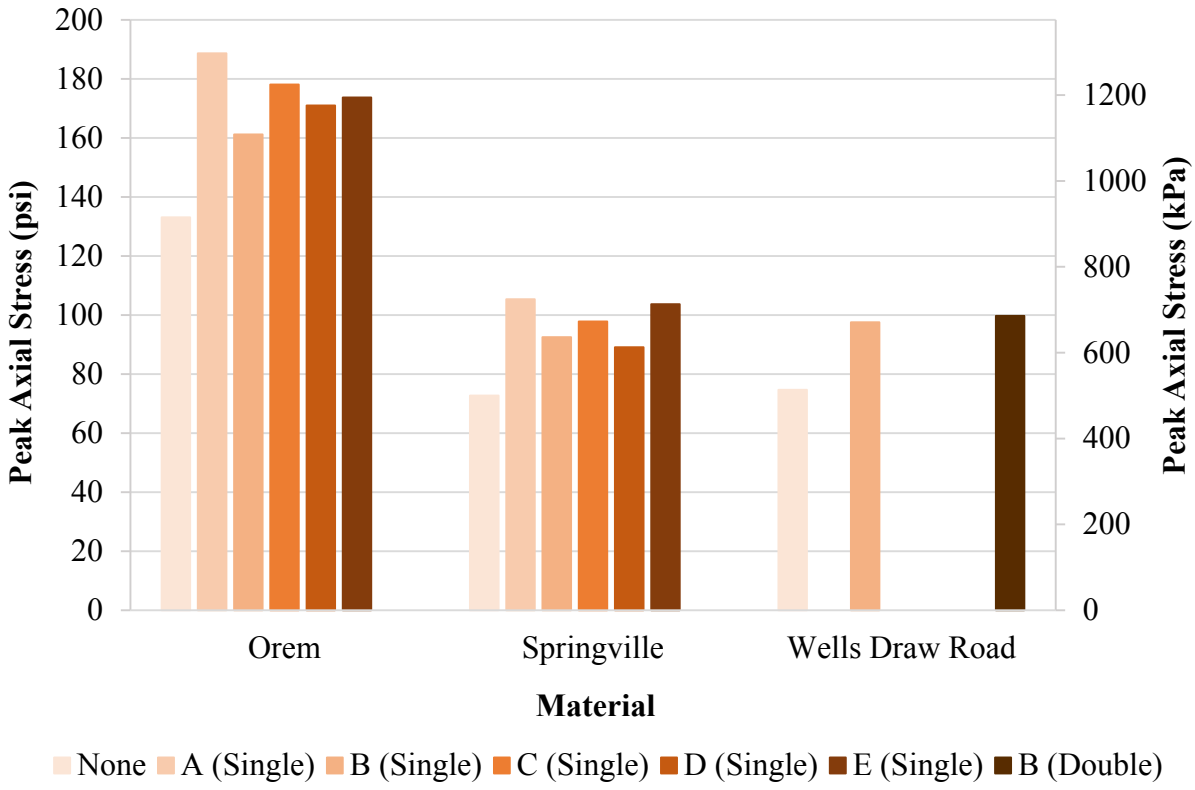

Figure 4-7: Least squares means for peak axial stress.

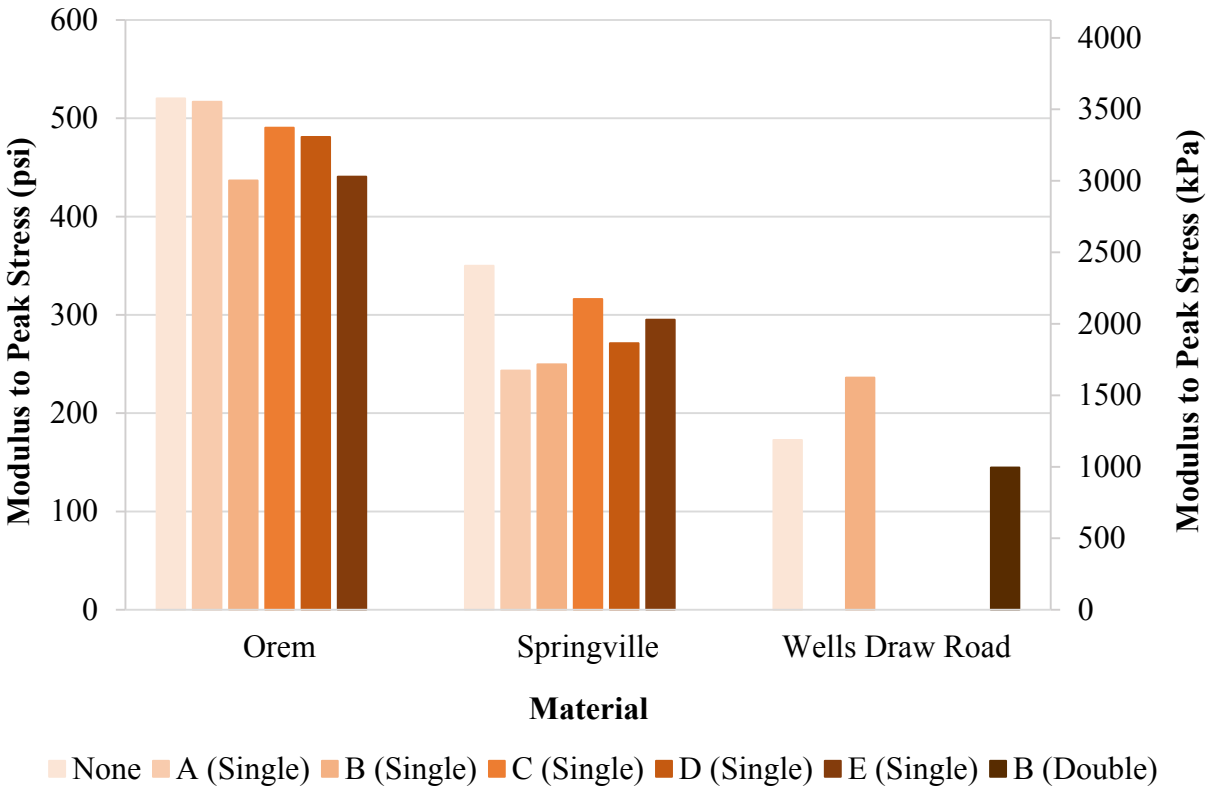

Figure 4-8: Least squares means for modulus to peak stress.

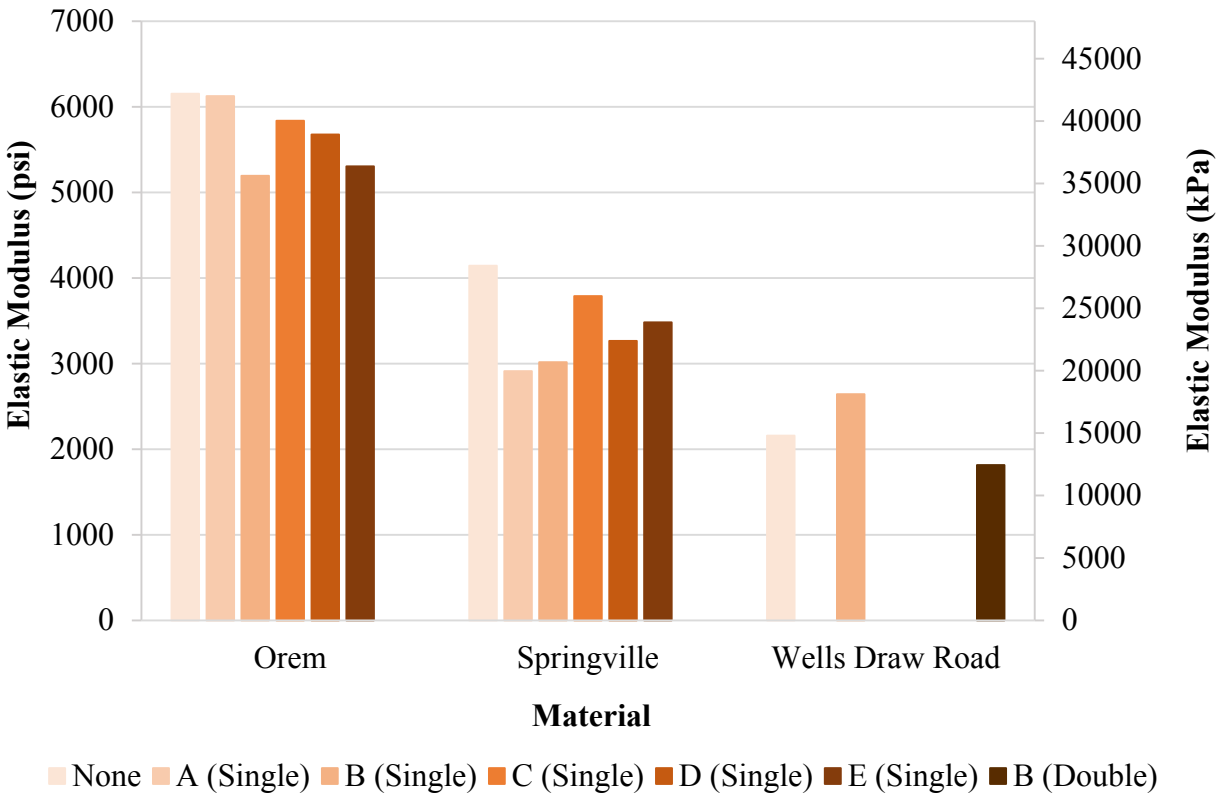

Figure 4-9: Least squares means for elastic modulus.

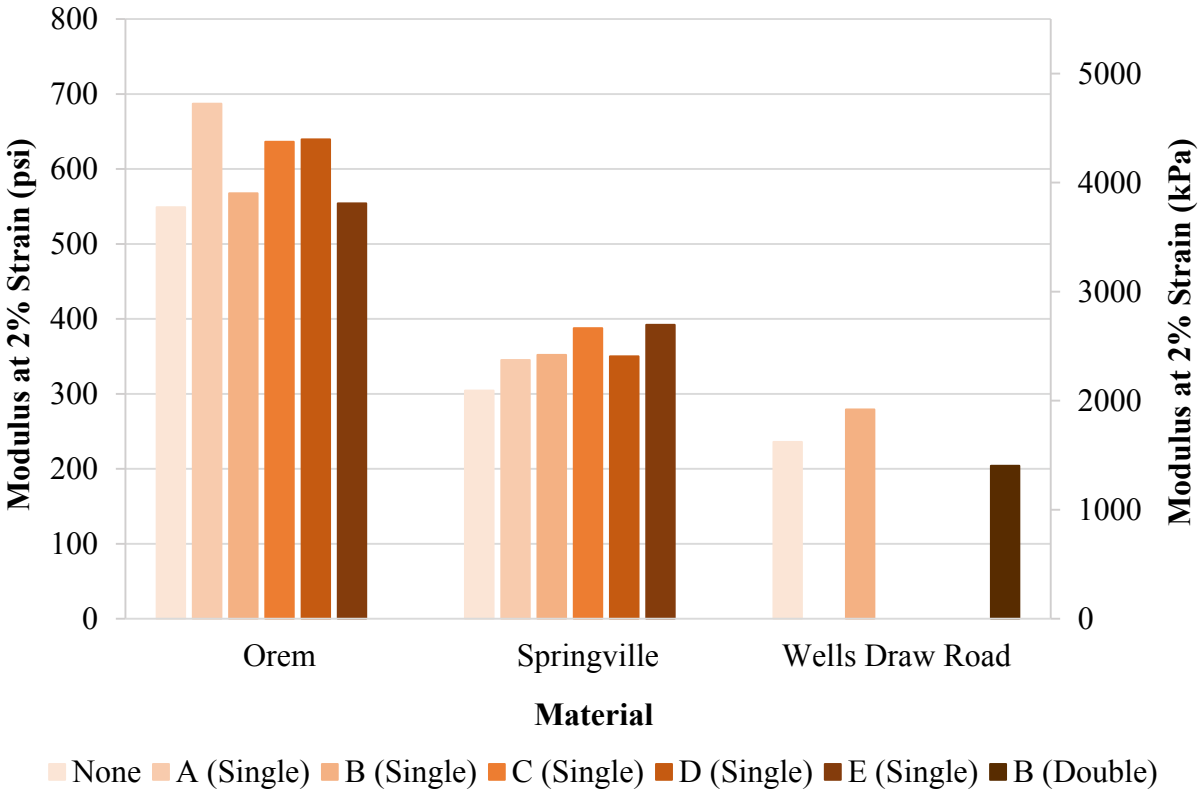

Figure 4-10: Least squares means for modulus at 2 percent strain.

for all possible comparisons, discussion is limited to the comparisons involving unstabilized control specimens.

Regarding peak axial stress, statistically significant differences between several of the geogrid-stabilized specimens and the unstabilized control specimens were observed for the Orem, Springville, and Wells Draw Road materials. Geogrid products A, B, C, D, and E increased the peak axial stress by an average of 42, 21, 34, 28, and 31 percent, respectively, for the Orem material, and geogrid products A, C, and E increased the peak axial stress by an average of 45, 35, and 43 percent, respectively, for the Springville material. For the Wells Draw Road material, the single- and double-layer geogrid configurations increased the peak axial stress

by an average of 31 and 34 percent, respectively. The differences in peak axial stress between geogrid-stabilized specimens and unstabilized control specimens were not statistically significant for geogrid products B or D for the Springville material.

Regarding modulus to peak stress, statistically significant differences between the geogrid-stabilized specimens and unstabilized control specimens were observed for the Wells Draw Road material. The single-layer geogrid configuration increased the modulus to peak stress by an average of 37 percent, while the double-layer geogrid configuration decreased the modulus to peak stress by an average of 16 percent. The differences in modulus to peak stress between geogrid-stabilized specimens and unstabilized control specimens were not statistically significant for geogrid product A, B, C, D, or E for the Orem or Springville material.

Regarding elastic modulus, statistically significant differences between the geogrid-stabilized specimens and unstabilized control specimens were not observed for the Orem, Springville, or Wells Draw Road material. The differences in elastic modulus between geogrid-stabilized specimens and unstabilized control specimens were not statistically significant for geogrid product A, B, C, D, or E for the Orem or Springville material or for the single- or double-layer geogrid configuration for the Wells Draw Road material.

Regarding modulus at 2 percent strain, a statistically significant difference between the geogrid-stabilized specimens and unstabilized control specimens was observed for the Orem material. Geogrid product A increased the modulus at 2 percent strain by an average of 25 percent for the Orem material. The differences in modulus at 2 percent strain between geogrid-stabilized specimens and unstabilized control specimens were not statistically significant for geogrid product B, C, D, or E for the Orem material; geogrid product A, B, C, D, or E for the

Springville material; or the single- or double-layer geogrid configuration for the Wells Draw Road material.

In summary, regarding peak axial stress, geogrid products A, B, C, D, and E led to statistically significant increases of 21 to 42 percent for the Orem material; geogrid products A, C, and E led to statistically significant increases of 35 to 45 percent for the Springville material; and the single- and double-layer configurations led to statistically significant increases of 31 to 34 percent for the Wells Draw Road material. Regarding modulus to peak stress, the single-layer geogrid configuration led to a statistically significant increase of 37 percent, while the double-layer geogrid configuration led to a statistically significant decrease of 16 percent for the Wells Draw Road material. Regarding elastic modulus, statistically significant differences between the geogrid-stabilized specimens and unstabilized control specimens were not observed for any of the geogrid products or configurations included in the study. Regarding modulus at 2 percent strain, geogrid product A led to a statistically significant increase of 25 percent for the Orem material. These results indicate that, regardless of the method of analysis, one geogrid product or configuration may be more effective than another at improving the structural quality of a given aggregate base material as measured using the quick shear test. As explained previously, further research is needed to determine which method of data analysis yields the best comparisons with field test results.

4.5 Summary

All results from this research are limited in their application to the aggregate base material types, geogrid products, and geogrid configurations associated with this study. The Orem material was classified as A-1-a and GW-GM (well-graded gravel with silt and sand), the

Springville material was classified as A-1-a and GW (well-graded gravel with sand), and the Wells Draw Road material was classified as A-1-a and GP-GM (poorly-graded gravel with silt and sand) according to the AASHTO and USCS methods, respectively.

The results of the ANOVAs performed to investigate differences between geogrid-stabilized specimens and unstabilized control specimens, without distinguishing among geogrid products or geogrid configurations, indicate that geogrid stabilization led to statistically significant increases of 31 to 34 percent in peak axial stress for all three materials, decreases of 17 to 18 percent in modulus to peak stress and elastic modulus for the Springville material, and an increase of 20 percent in modulus at 2 percent strain for the Springville material. Therefore, depending on the method of data analysis, the quick shear test results indicate that geogrid stabilization, with the effect of geogrid stabilization averaged across all of the geogrid products evaluated in this study, may or may not improve the structural quality of the aggregate base materials evaluated in this study.

The results of the ANOVAs performed to investigate differences between individual geogrid products or geogrid configurations also depended on the method of data analysis. Regarding peak axial stress, geogrid products A, B, C, D, and E led to statistically significant increases of 21 to 42 percent for the Orem material; geogrid products A, C, and E led to statistically significant increases of 35 to 45 percent for the Springville material; and the single- and double-layer configurations led to statistically significant increases of 31 to 34 percent for the Wells Draw Road material. Regarding modulus to peak stress, the single-layer geogrid configuration led to a statistically significant increase of 37 percent, while the double-layer geogrid configuration led to a statistically significant decrease of 16 percent for the Wells Draw Road material. Regarding elastic modulus, statistically significant differences between the

geogrid-stabilized specimens and unstabilized control specimens were not observed for any of the geogrid products or configurations included in the study. Regarding modulus at 2 percent strain, geogrid product A led to a statistically significant increase of 25 percent for the Orem material. These results indicate that, regardless of the method of analysis, one geogrid product or configuration may be more effective than another at improving the structural quality of a given aggregate base material as measured using the quick shear test. Further research is needed to determine which method of data analysis yields the best comparisons with field test results.

5 CONCLUSION

5.1 Summary

The objective of this research was to apply a previously recommended laboratory testing protocol to specific aggregate base materials that are also the subject of ongoing full-scale field testing. The scope of this research involved three aggregate base materials selected from three sites where full-scale field testing programs have been established. The first and second field sites included five different geogrid types, categorized as either BX or TX, in a single-layer configuration, while the third site included only the TX geogrid type in either a single- or double-layer configuration. To ensure a direct comparison between laboratory and field test results, the same geogrid products that were used at the field sites were also used in the laboratory testing.

Geogrid-stabilized and unstabilized control specimens were evaluated using the AASHTO T 307 quick shear testing protocol. Measurements of load and axial displacement were recorded and used to develop a stress-strain plot for each specimen tested. The peak axial stress, the modulus to the peak axial stress, the modulus of the elastic portion of the curve, and the modulus at 2 percent strain were then calculated. After the testing, the gravimetric moisture content and dry density of each specimen were calculated. Statistical analyses were then performed to investigate differences between geogrid-stabilized specimens and unstabilized control specimens and to investigate differences between individual geogrid products or geogrid

configurations. (The intent of the analysis was not to suggest that a given geogrid product is generally better than another but rather to investigate the differences in compatibility of the different geogrid products with the specific aggregate base materials included in this research.)

5.2 Findings

All results from this research are limited in their application to the aggregate base material types, geogrid products, and geogrid configurations associated with this study. The Orem material was classified as A-1-a and GW-GM (well-graded gravel with silt and sand), the Springville material was classified as A-1-a and GW (well-graded gravel with sand), and the Wells Draw Road material was classified as A-1-a and GP-GM (poorly-graded gravel with silt and sand) according to the AASHTO and USCS methods, respectively.

The results of the ANOVAs performed to investigate differences between geogrid-stabilized specimens and unstabilized control specimens, without distinguishing among geogrid products or geogrid configurations, indicate that geogrid stabilization led to statistically significant increases of 31 to 34 percent in peak axial stress for all three materials, decreases of 17 to 18 percent in modulus to peak stress and elastic modulus for the Springville material, and an increase of 20 percent in modulus at 2 percent strain for the Springville material. Therefore, depending on the method of data analysis, the quick shear test results indicate that geogrid stabilization, with the effect of geogrid stabilization averaged across all of the geogrid products evaluated in this study, may or may not improve the structural quality of the aggregate base materials evaluated in this study.

The results of the ANOVAs performed to investigate differences between individual geogrid products or geogrid configurations also depended on the method of data analysis.

Regarding peak axial stress, geogrid products A, B, C, D, and E led to statistically significant increases of 21 to 42 percent for the Orem material; geogrid products A, C, and E led to statistically significant increases of 35 to 45 percent for the Springville material; and the single- and double-layer configurations led to statistically significant increases of 31 to 34 percent for the Wells Draw Road material. Regarding modulus to peak stress, the single-layer geogrid configuration led to a statistically significant increase of 37 percent, while the double-layer geogrid configuration led to a statistically significant decrease of 16 percent for the Wells Draw Road material. Regarding elastic modulus, statistically significant differences between the geogrid-stabilized specimens and unstabilized control specimens were not observed for any of the geogrid products or configurations included in the study. Regarding modulus at 2 percent strain, geogrid product A led to a statistically significant increase of 25 percent for the Orem material. These results indicate that, regardless of the method of analysis, one geogrid product or configuration may be more effective than another at improving the structural quality of a given aggregate base material as measured using the quick shear test.

5.3 Recommendations

Additional research is needed to compare the results of the laboratory quick shear testing obtained for this study with the structural capacity of the geogrid-stabilized and unstabilized control sections that have been constructed at corresponding full-scale field testing sites. Specifically, further research is needed to determine which method of laboratory data analysis yields the best comparisons with field test results. Depending on the results of those comparisons, the equivalent of a conditioning period, or a period of trafficking and densification that occurs in the field before the full effects of geogrid stabilization can be observed, may be

appropriately introduced in the laboratory to enable better predictions of field performance. Finally, correlations between the results of quick shear testing and resilient modulus need to be investigated in order to incorporate the findings of the quick shear test on geogrid-stabilized base materials into mechanistic-empirical pavement design.

REFERENCES

Abu-Farsakh, M., Souci, G., Voyiadjis, G. Z., and Chen, Q. (2012). "Evaluation of factors affecting the performance of geogrid-reinforced granular base material using repeated load triaxial tests." *Journal of Materials in Civil Engineering*, 24(1), 72-83.

Al-Qadi, I. L., Brandon, T. L., and Bhutta, S. A. (1997). "Geosynthetic stabilized flexible pavements." *Proceedings of Geosynthetics '97*, Industrial Fabrics Association International (IFAI), Roseville, MN, 647-662.

Al-Qadi, I. L., Dessouky, S. H., Kwon, J., and Tutumluer, E. (2008). "Geogrid in flexible pavements: validated mechanism." *Transportation Research Record: Journal of the Transportation Research Board*, 2045, 102-109.

American Association of State Highway and Transportation Officials (AASHTO) (2008). "Mechanistic-empirical pavement design guide: a manual of practice." Washington, DC.

Aran, S. (2006). "Base reinforcement with biaxial geogrid: long-term performance." *Transportation Research Record: Journal of the Transportation Research Board*, 1975, 115-123.

Brown, S. F., Kwan, J., and Thom, N. H. (2007). "Identifying the key parameters that influence geogrid reinforcement of railway ballast." *Geotextiles and Geomembranes*, 25(6), 326-335.

Cancelli, A., and Montanelli, F. (1999). "In-ground test for geosynthetic reinforced flexible paved roads." *Proceedings of the Conference Geosynthetics '99*, IFAI, Roseville, MN, 863-878.

Chen, Q., and Abu-Farsakh, M. (2012). "Structural contribution of geogrid reinforcement in pavement." *GeoCongress 2012: State of the Art and Practice in Geotechnical Engineering*, ASCE, Reston, VA, 1468-1475.

Federal Highway Administration (FHWA). (2008). "Geosynthetic design and construction guidelines." Report No. FHWA NHI-07-092, FHWA, United States Department of Transportation, McLean, VA.

Haas, R., Walls, J., and Carroll, R. G. (1988). "Geogrid reinforcement of granular bases in flexible pavements." *Transportation Research Record: Journal of the Transportation Research Board*, 1188, 19-27.

Hall, K. D., Warren, K. A., and Howard, I. L. (2004). "Low volume flexible pavement roads reinforced with geosynthetics." Final Report AHTD TRC-0406, Planning and Research Division, Arkansas State Highway and Transportation Department, Little Rock, AR.

Hanes Geo Components. (2015). "Terragrid RX 1200 product data sheet." <http://hanesgeo.com/Catalog/Product?id=1704> (December 15, 2015).

Hatami, K., Mahmood, T., Zaman, M., and Ghabchi, R. (2012). "Development of ODOT guidelines for the use of geogrids in aggregate bases." Report No. OTCREOS9.1-23-F, Oklahoma Transportation Center, Midwest City, OK.

Hilton, S. T. (2017). "Full-scale pavement testing of aggregate base material stabilized with triaxial geogrid." M.S. thesis, Department of Civil and Environmental Engineering, Brigham Young University, Provo, UT.

Huntington, G., and Ksaibati, K. (2000). "Evaluation of geogrid-reinforced granular base." *Geotechnical Fabrics Report*, 18(1), 22-28.

Knighton, J. T. (2015). "Investigation of laboratory test procedures for assessing the structural capacity of geogrid-reinforced aggregate base materials." M.S. thesis, Department of Civil and Environmental Engineering, Brigham Young University, Provo, UT.

Kwon, J., and Tutumluer, E. (2009). "Geogrid base reinforcement with aggregate interlock and modeling of associated stiffness enhancement in mechanistic pavement analysis." *Transportation Research Record: Journal of the Transportation Research Board*, 2116, 85-95.

Kwon, J., Tutumluer, E., Al-Qadi, I., and Dessouky, S. (2008). "Effectiveness of geogrid base-reinforcement in low-volume flexible pavements." *GeoCongress 2008: Geosustainability and Geohazard Mitigation*, ASCE, Reston, VA.

Moghaddas-Nejad, F., and Small, J. C. (2003). "Resilient and permanent characteristics of reinforced granular materials by repeated load triaxial tests." *Geotechnical Testing Journal*, 26(2), 152-166.

Montanelli, F., Zhao, A., and Rimoldi, P. (1997). "Geosynthetic-reinforced pavement system: testing and design." *Proceedings of the Conference Geosynthetics '97*, IFAI, Roseville, MN, 619-632.

Nazzal, M., Abu-Farsakh, M., and Mohammad, L. (2007). "Evaluation of geogrid benefits using monotonic and repeated load triaxial tests." *Analysis of Asphalt Pavement Materials and Systems*, 145-155.

National Cooperative Highway Research Program (NCHRP) (2004a). "Guide for mechanistic-empirical design of new and rehabilitated structures." NCHRP Report 1-37A, Transportation Research Board, Washington, DC.

NCHRP (2004b). "Laboratory determination of resilient modulus for flexible pavement design." NCHRP Report 1-28A, Transportation Research Board, Washington, DC.

National Highway Institute (NHI) (2002). "Introduction to mechanistic-empirical pavement design: reference manual." Report No. NHI-02-048, Arlington, VA.

Perkins, S. W., and Ismeik, M. A. (1997). "A synthesis and evaluation of geosynthetic-reinforced base layers in flexible pavements: part I. *Geosynthetics International*, (4)6, 549-604.

Perkins, S. W. (1999). "Geosynthetic reinforcement of flexible pavements: laboratory based pavement test sections." Report No. FHWA/MT-99-001/8138, FHWA, United States Department of Transportation, Washington, DC.

Perkins, S. W., Christopher, B. R., Cuelho, E. L., Eiksund, G. R., Hoff, I., Schwartz, C. W., Svanø, G., and Watn, A. (2004). "Development of design methods for geosynthetic-reinforced flexible pavements." Report No. DTFH61-01-X-00068, FHWA, United States Department of Transportation, Washington, DC.

Qian, Y., Han, J., Pokharel, S., and Parsons, R. (2013). "Performance of triangular aperture geogrid-reinforced base courses over weak subgrade under cyclic loading." *Journal of Materials in Civil Engineering*, 25(8), 1013-1021.

Rahman, M., Arulrajah, A., Piratheepan, J., Bo, M., and Imteaz, M. (2014). "Resilient modulus and permanent deformation responses of geogrid-reinforced construction and demolition materials." *Journal of Materials in Civil Engineering*, 26(3), 512-519.

Reck, N. C. (2009). "Mechanistic empirical design of geogrid reinforced paved flexible pavements." *Proceedings of Jubilee Symposium on Polymer Geogrid Reinforcement*, Institute of Civil Engineers, London, England.

Sweat, E. J (2016). "Investigation of structural capacity of geogrid-reinforced aggregate base materials in flexible pavements." M.S. thesis, Department of Civil and Environmental Engineering, Brigham Young University, Provo, UT.

Tang, X., Stoffels, S. M., and Palomino, A. M. (2013). "Resilient and permanent deformation characteristics of unbound pavement layers modified by geogrids." *Transportation Research Record: Journal of the Transportation Research Board*, 2369, 3-10.

Tensar International Corporation. (2015). "Biaxial (BX) geogrid product specification sheet." <http://www.tensarcorp.com/Systems-and-Products/Tensar-geogrids/Tensar-Biaxial-BX-geogrids> (December 15, 2015).

Tingle, J. S., and Jersey, S. R. (2009). "Full-scale evaluation of geosynthetic-reinforced aggregate roads." *Transportation Research Record: Journal of the Transportation Research Board*, 2116, 96-107.

Tutumluer, E., and Kwon, J. (2006). "Evaluation of geosynthetics use for pavement subgrade restraint and working platform construction." *ASCE Geotechnical Practice Publication No. 3: Geotechnical Applications for Transportation Infrastructure*, Titi, H., eds., ASCE, Reston, VA, 96-107.

Wayne, M., Boudreau R. L., and Kwon, J. (2011a). "Characterization of mechanically stabilized layer by resilient modulus and permanent deformation testing. *Transportation Research Record: Journal of the Transportation Research Board*, 2204, 76-82.

Wayne, M. H., Kwon, J., and Boudreau, R. (2011b). "Resilient modulus, repeated load permanent deformation and plate load testing of a mechanically stabilized crushed miscellaneous base material." *Transportation Research Board 90th Annual Meeting*, Washington, DC.

Xiao, Y., Tutumluer, E., Qian, Y., and Siekmeier, J. A. (2012). "Gradation effects influencing mechanical properties of aggregate base-granular subbase materials in Minnesota." *Transportation Research Record: Journal of the Transportation Research Board*, 2267, 14-26.

APPENDIX A MOISTURE-DENSITY RELATIONSHIPS

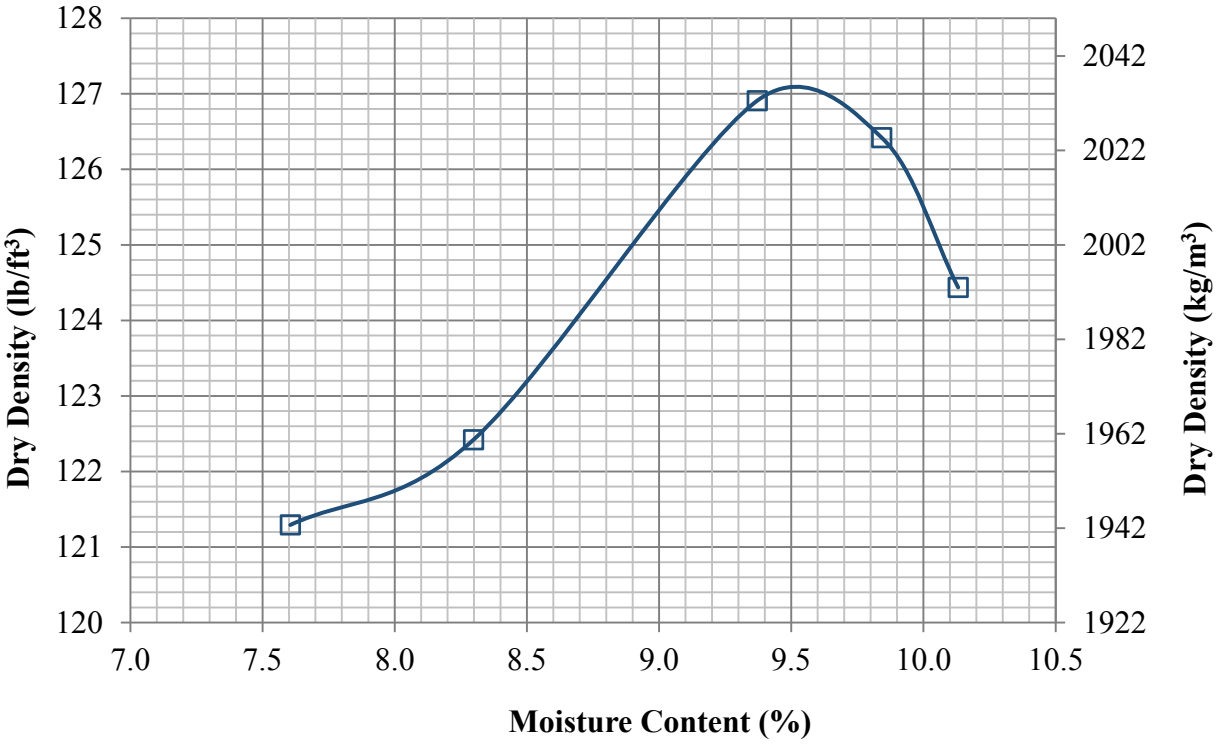

Figure A-1: Moisture-density curve for Orem material.

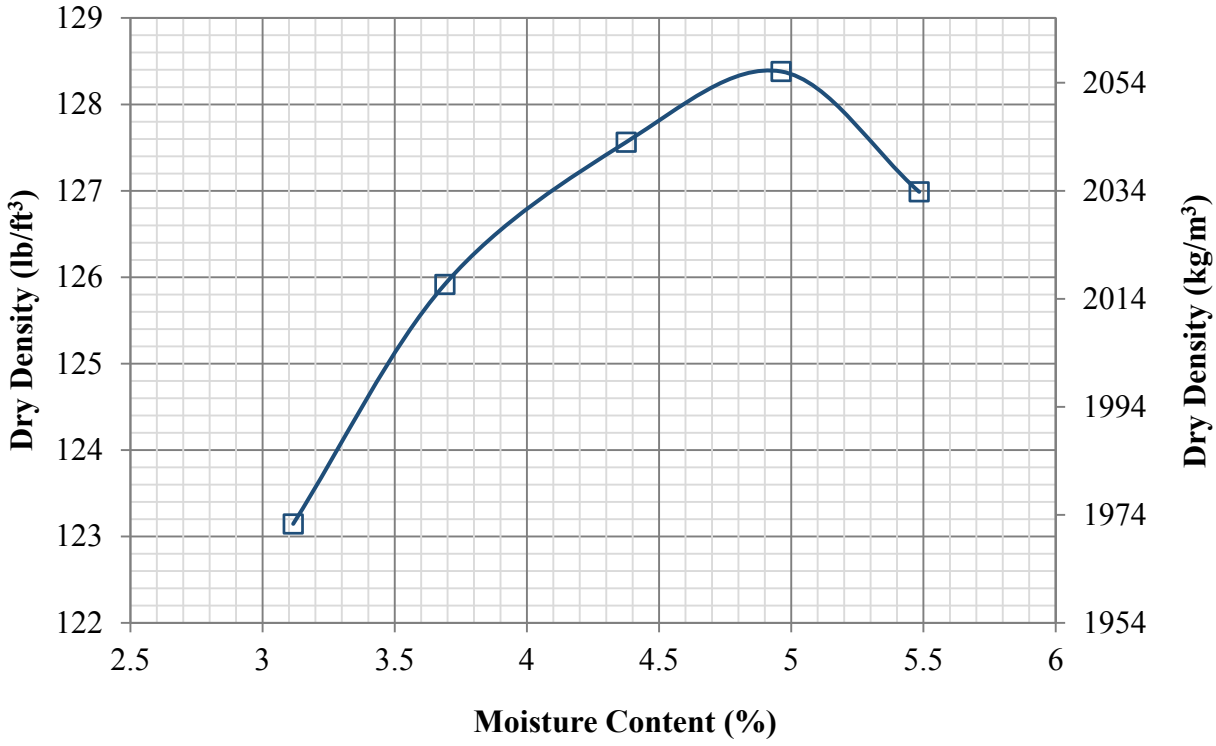

Figure A-2: Moisture-density curve for Springville material.

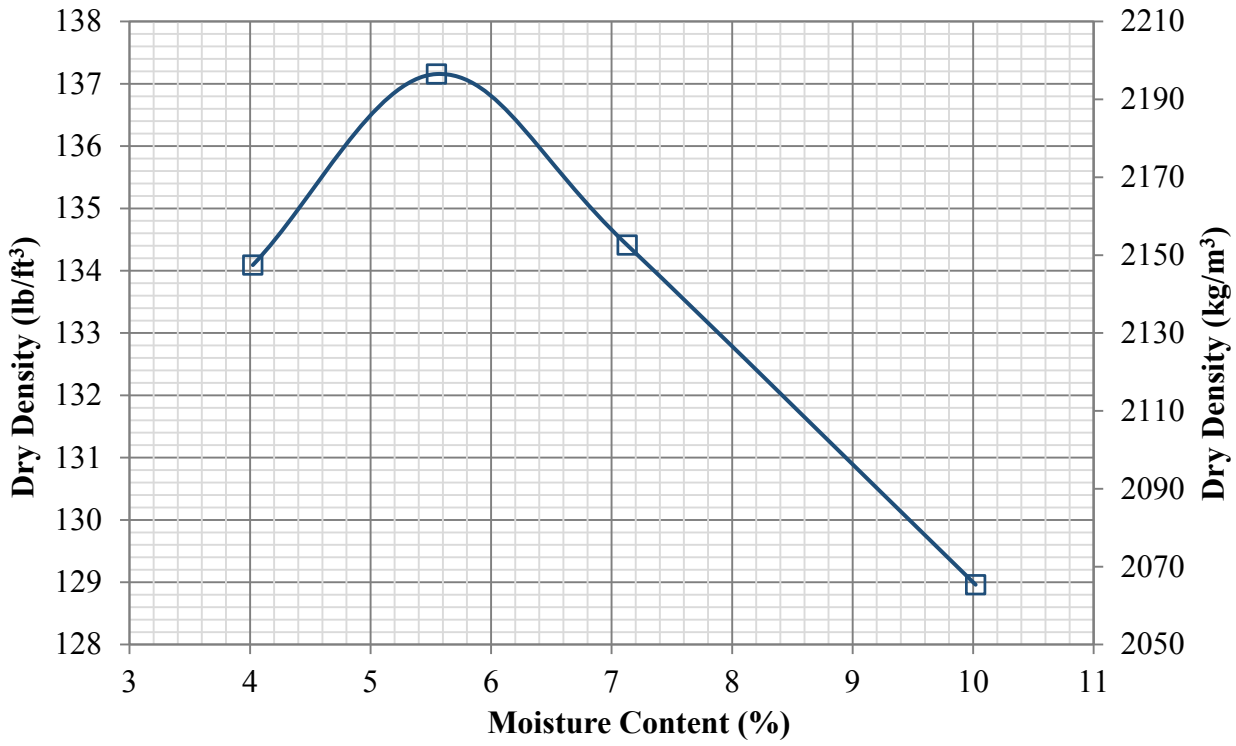

Figure A-3: Moisture-density curve for Wells Draw Road material.

APPENDIX B MECHANICAL PROPERTY TEST DATA

Table B-1: Quick Shear Test Data

Material	Geogrid Product	Specimen	Height, in. (mm)		Weight, lb (kg)		Moisture Content, %	Estimated Dry Density, lb/ft^3 (kg/m^3)		Percent MDD, %	Peak Axial Stress, psi (kPa)		Modulus to Peak Stress, psi (kPa)		Elastic Modulus, psi (kPa)		Modulus at 2% Strain, psi (kPa)	
Orem	None	1	11.8	(301)	26.8	(12.15)	8.7	126.7	(2030)	99.7	134.0	(924)	548.9	(3785)	6496.7	(44793)	557.1	(3841)
		2	11.8	(300)	26.3	(11.93)	8.6	126.1	(2020)	99.2	132.3	(912)	491.4	(3388)	5811.5	(40069)	540.9	(3729)
	A	1	11.8	(300)	26.5	(12.03)	8.6	126.1	(2020)	99.2	191.7	(1322)	536.1	(3696)	6325.8	(43615)	707.5	(4878)
		2	11.9	(303)	26.7	(12.09)	8.4	125.1	(2003)	98.4	185.6	(1280)	497.5	(3430)	5927.2	(40866)	666.5	(4595)
	B	1	11.9	(301)	26.5	(12.02)	8.7	125.3	(2008)	98.6	155.8	(1074)	458.1	(3158)	5435.3	(37475)	587.9	(4054)
		2	11.9	(303)	26.7	(12.10)	8.5	125.7	(2014)	98.9	166.7	(1149)	415.5	(2865)	4951.7	(34141)	547.4	(3774)
	C	1	11.8	(301)	26.5	(12.02)	8.5	125.6	(2012)	98.8	177.5	(1224)	492.5	(3396)	5833.9	(40223)	636.0	(4385)
		2	12.0	(304)	26.7	(12.10)	8.6	125.2	(2005)	98.5	178.7	(1232)	488.3	(3367)	5842.3	(40281)	636.4	(4388)
	D	1	11.8	(300)	26.4	(11.98)	8.5	125.7	(2014)	98.9	174.6	(1204)	514.8	(3550)	6073.8	(41878)	669.8	(4618)
		2	11.8	(300)	26.4	(11.97)	8.5	125.5	(2011)	98.8	167.5	(1155)	447.2	(3084)	5278.6	(36395)	609.3	(4201)
	E	1	11.8	(301)	26.9	(12.19)	8.6	126.3	(2023)	99.4	176.5	(1217)	463.3	(3194)	5485.7	(37823)	570.2	(3931)
		2	12.2	(311)	27.2	(12.36)	8.5	124.8	(1999)	98.2	170.9	(1178)	418.2	(2883)	5122.8	(35321)	538.2	(3711)
Springville	None	1	11.7	(298)	27.2	(12.35)	4.4	135.1	(2164)	105.2	79.4	(548)	374.6	(2583)	4396.1	(30310)	331.9	(2288)
		2	11.9	(302)	27.2	(12.33)	4.5	132.9	(2130)	103.5	66.0	(455)	325.5	(2244)	3871.2	(26691)	276.9	(1909)
	A	1	11.9	(302)	27.3	(12.37)	4.3	133.6	(2140)	104.0	106.4	(733)	230.8	(1591)	2742.9	(18912)	308.8	(2129)
		2	12.0	(306)	27.5	(12.49)	4.4	133.1	(2132)	103.7	104.4	(720)	255.9	(1764)	3080.8	(21242)	381.7	(2632)
	B	1	12.1	(308)	27.6	(12.54)	4.3	132.7	(2126)	103.3	94.1	(649)	241.6	(1666)	2930.1	(20203)	353.9	(2440)
		2	12.0	(305)	27.6	(12.51)	4.4	133.5	(2138)	104.0	90.9	(627)	258.0	(1779)	3101.8	(21387)	350.2	(2414)
	C	1	12.1	(307)	27.8	(12.62)	4.5	133.8	(2143)	104.2	93.0	(641)	343.8	(2371)	4160.0	(28682)	377.8	(2605)
		2	11.8	(301)	27.2	(12.35)	4.5	133.7	(2141)	104.1	102.6	(708)	288.3	(1988)	3416.3	(23554)	397.5	(2741)
	D	1	11.9	(303)	27.1	(12.31)	4.4	132.3	(2119)	103.0	87.5	(603)	257.6	(1776)	3075.5	(21205)	342.1	(2359)
		2	12.1	(308)	28.0	(12.70)	4.5	134.4	(2153)	104.7	90.7	(625)	284.9	(1965)	3455.1	(23822)	357.8	(2467)
	E	1	11.8	(300)	27.3	(12.38)	4.4	134.7	(2158)	104.9	101.9	(703)	317.9	(2192)	3749.1	(25849)	402.8	(2777)
		2	11.8	(300)	27.4	(12.41)	4.4	134.8	(2159)	105.0	105.5	(727)	272.4	(1878)	3215.7	(22171)	381.4	(2630)
Wells Draw Road	None	1	12.0	(305)	29.1	(13.21)	5.6	140.6	(2252)	102.5	74.8	(515)	182.5	(1258)	2190.2	(15101)	229.8	(1585)
		2	11.8	(300)	28.7	(13.00)	5.6	140.7	(2253)	102.5	79.2	(546)	180.3	(1243)	2127.0	(14665)	242.1	(1669)
	B (Single)	1	12.0	(305)	29.1	(13.21)	5.7	140.3	(2248)	102.3	97.4	(671)	235.3	(1622)	2828.4	(19501)	306.6	(2114)
		2	11.9	(301)	28.8	(13.05)	6.4	140.4	(2249)	102.3	95.6	(659)	207.2	(1429)	2458.2	(16949)	251.7	(1735)
	B (Double)	1	12.0	(305)	29.0	(13.14)	5.5	139.7	(2239)	101.9	91.3	(629)	143.7	(991)	1724.6	(11891)	214.8	(1481)
		2	12.0	(305)	29.0	(13.15)	5.6	139.5	(2234)	101.7	105.8	(729)	158.4	(1092)	1902.6	(13118)	193.4	(1334)

Table B-1: Omitted Quick Shear Test Data

Material	Geogrid Product	Specimen	Height, in. (mm)		Weight, lb (kg)		Moisture Content, %	Estimated Dry Density, pcf (kg/m^3)		Percent MDD (%)	Peak Axial Stress, psi (kPa)		Modulus to Peak Stress, psi (kPa)		Elastic Modulus, psi (kPa)		Modulus at 2% Strain, psi (kPa)	
Orem	B	1	11.9	(302)	26.7	(12.11)	8.5	126.0	(2018)	99.1	404.1	(2786)	1143.5	(7884)	13608.4	(93826)	1430.9	(9866)
Springville	E	2	11.9	(303)	27.2	(12.34)	4.5	132.7	(2126)	103.3	93.7	(646)	228.6	(1576)	2728.3	(18811)	349.2	(2407)
Wells Draw Road	B (Double)	2	11.8	(300)	28.8	(13.05)	5.5	140.9	(2258)	102.7	111.2	(766)	206.8	(1426)	2446.1	(16866)	279.2	(1925)

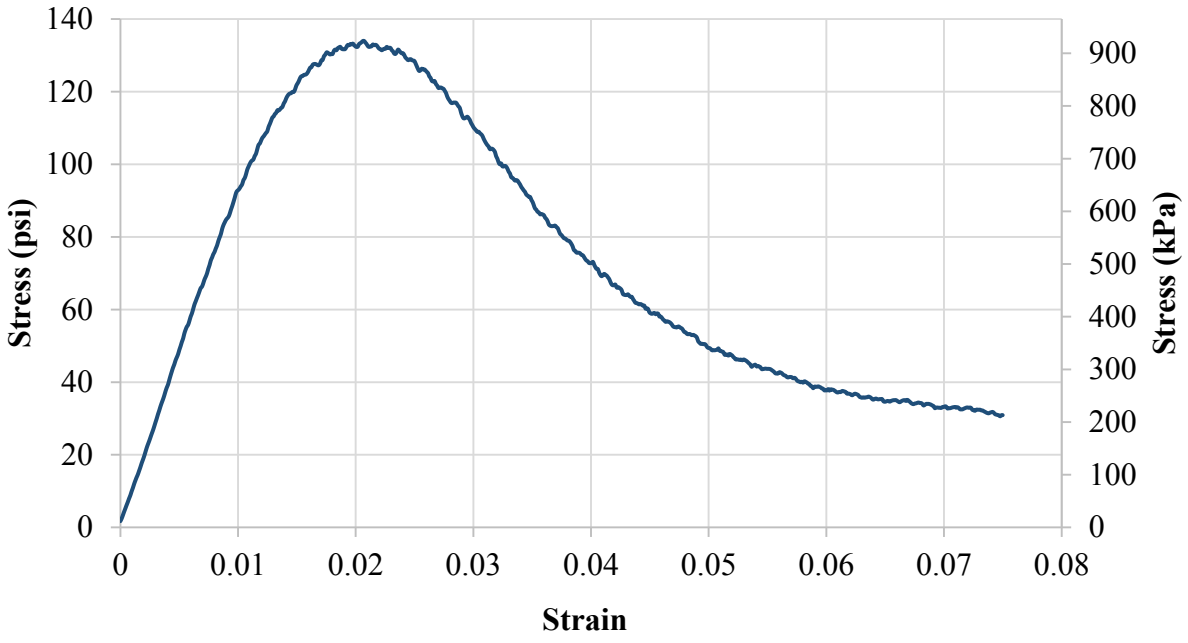

(a)

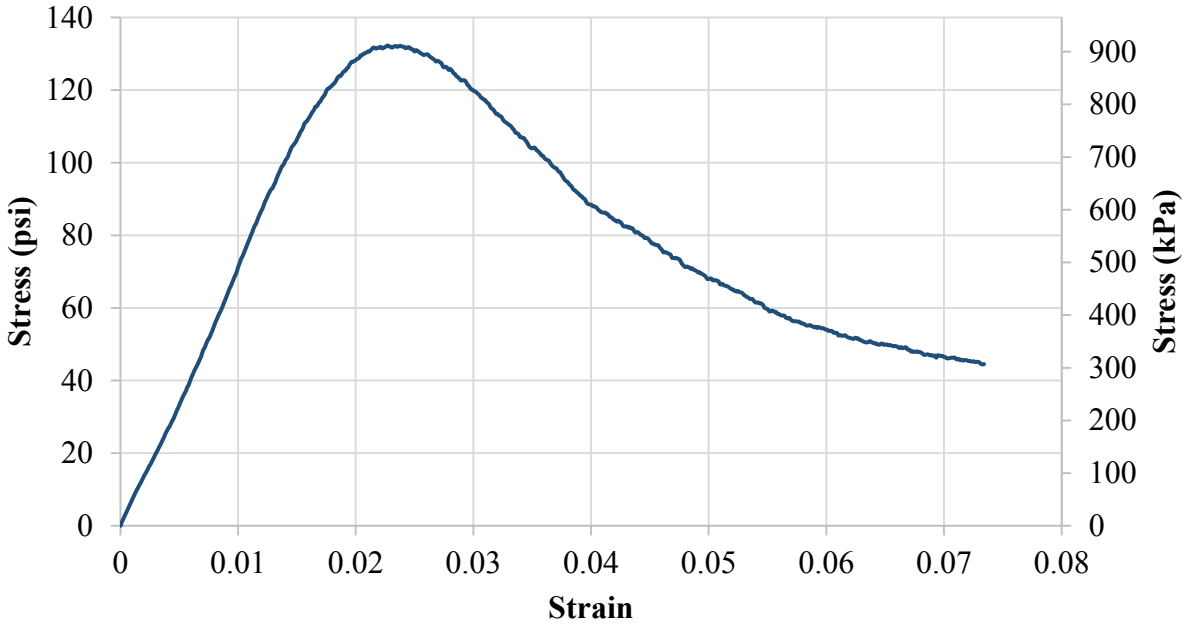

(b)

Figure B-1: Stress-strain plot for unstabilized Orem base material: (a) specimen 1 and (b) specimen 2.

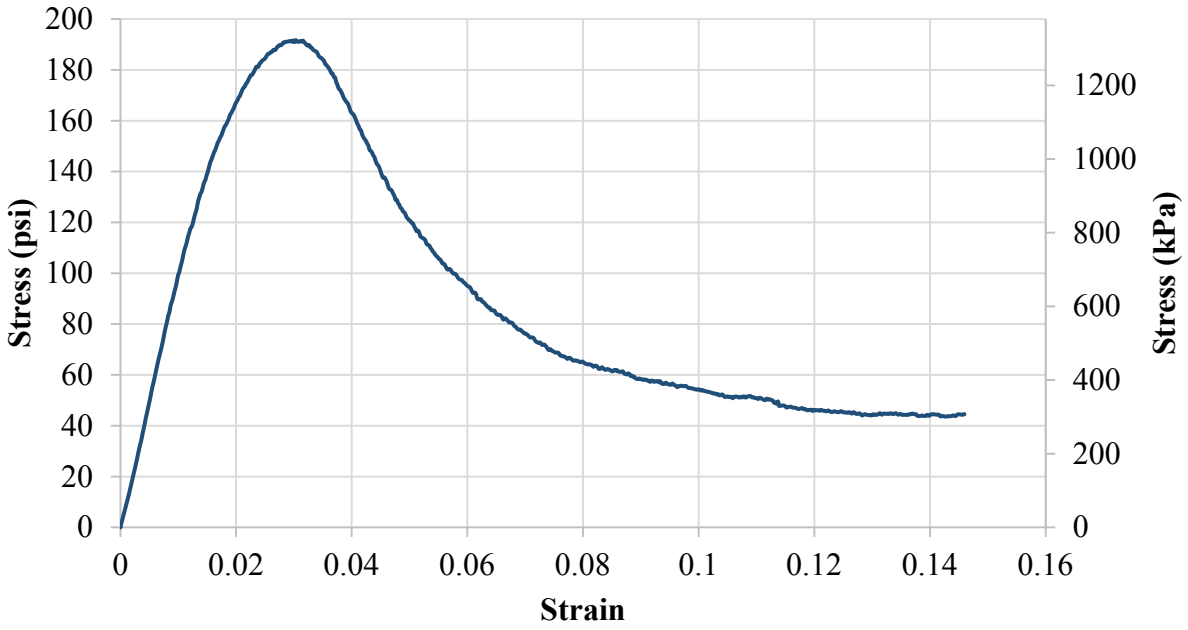

(a)

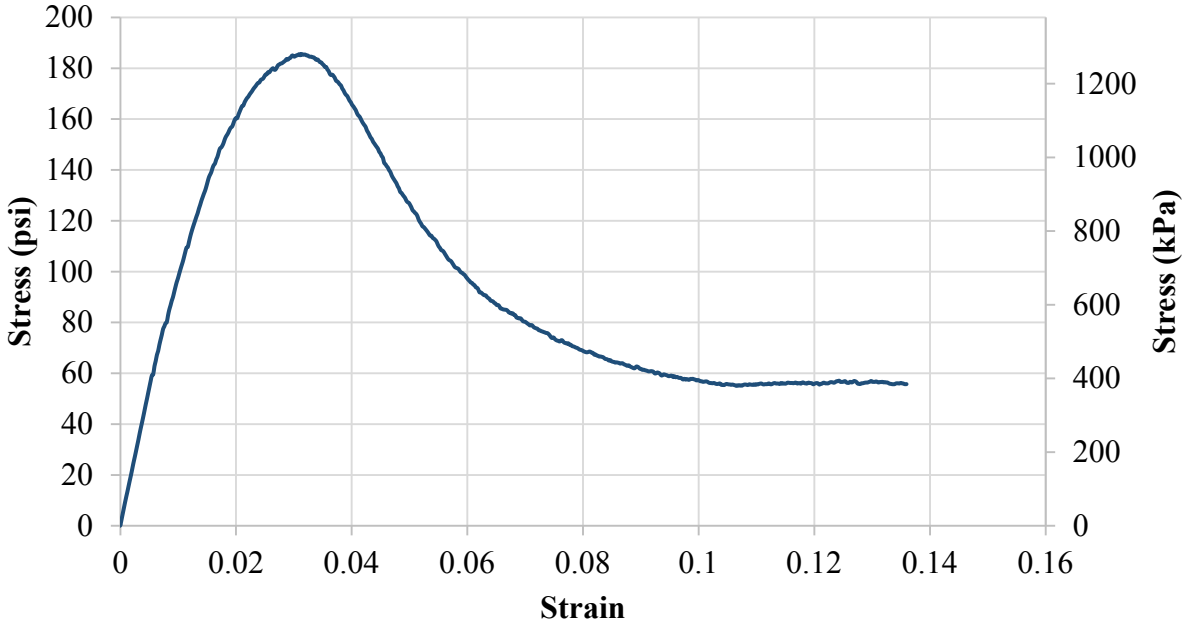

(b)

Figure B-2: Stress-strain plot for Orem base material stabilized with geogrid product A: (a) specimen 1 and (b) specimen 2.

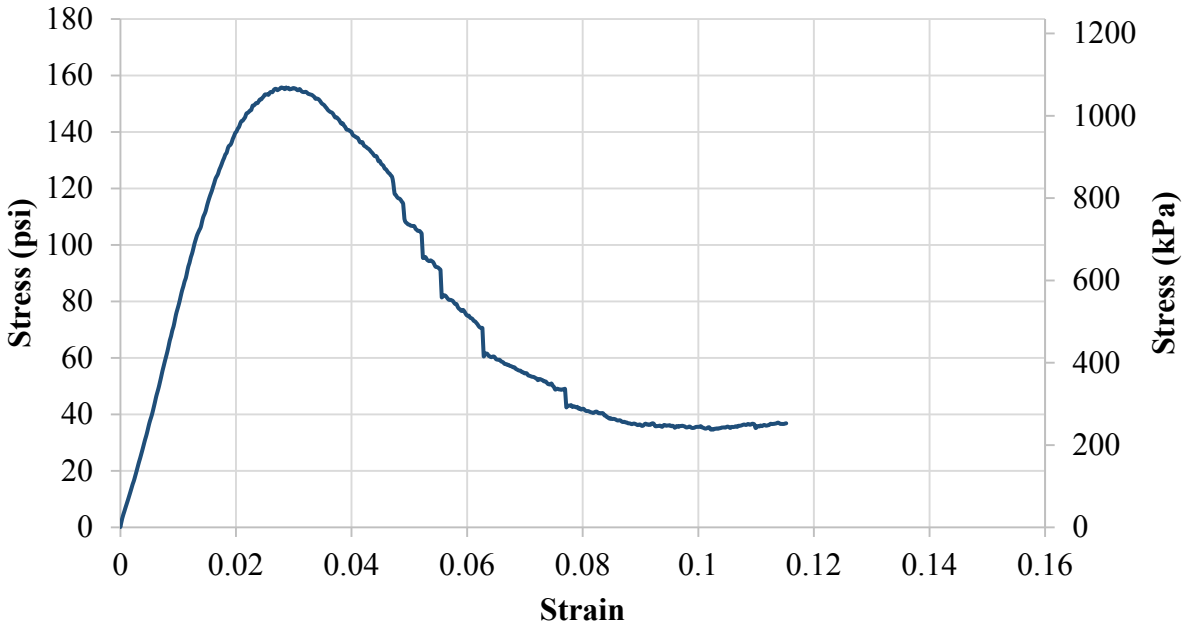

(a)

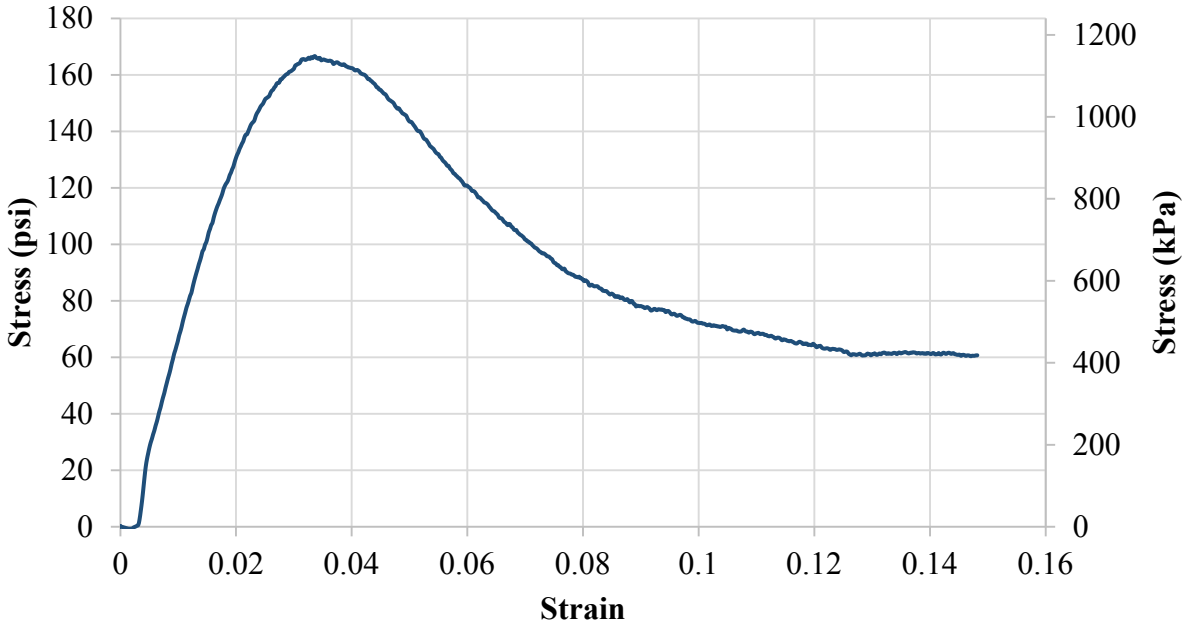

(b)

Figure B-3: Stress-strain plot for Orem base material stabilized with geogrid product B: (a) specimen 1 and (b) specimen 2.

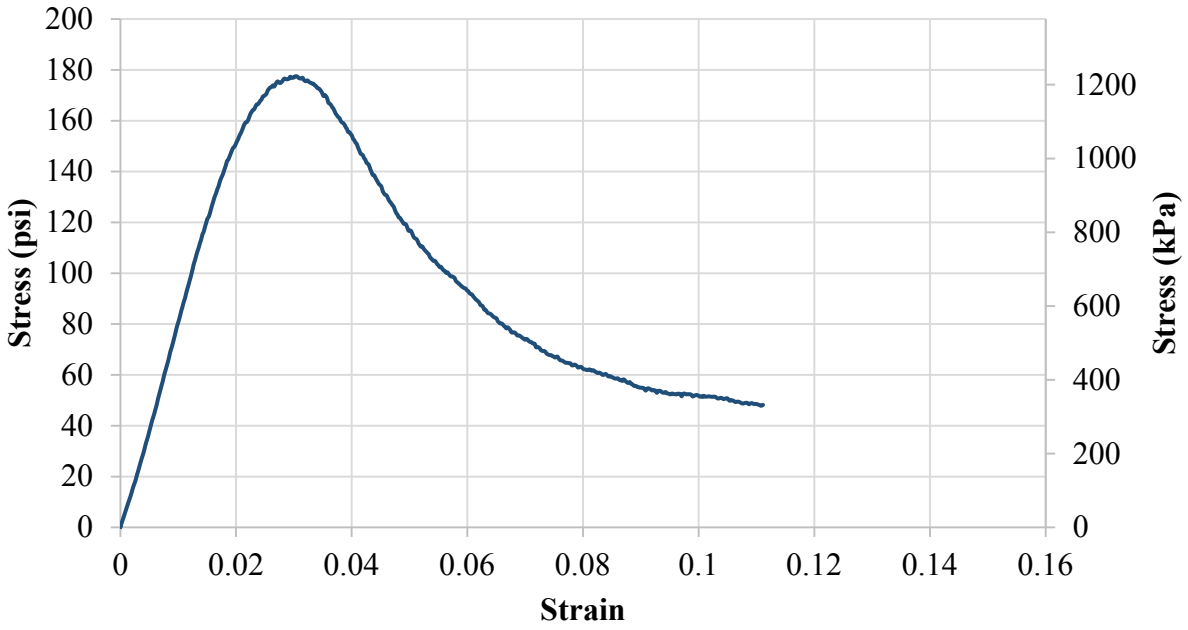

(a)

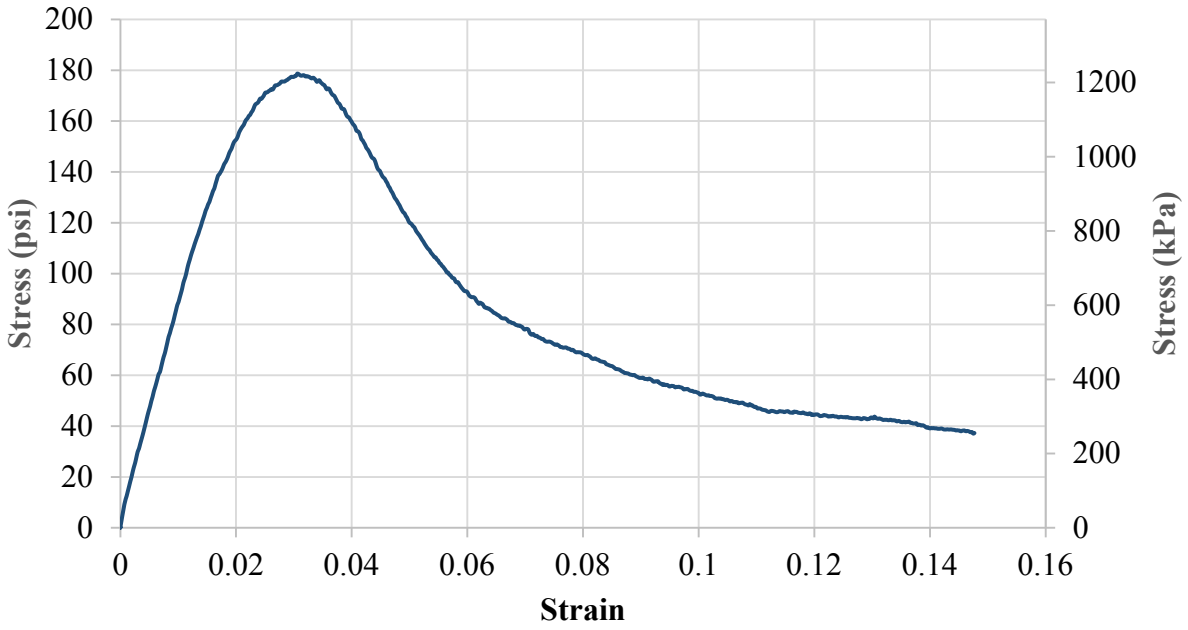

(b)

Figure B-4: Stress-strain plot for Orem base material stabilized with geogrid product C: (a) specimen 1 and (b) specimen 2.

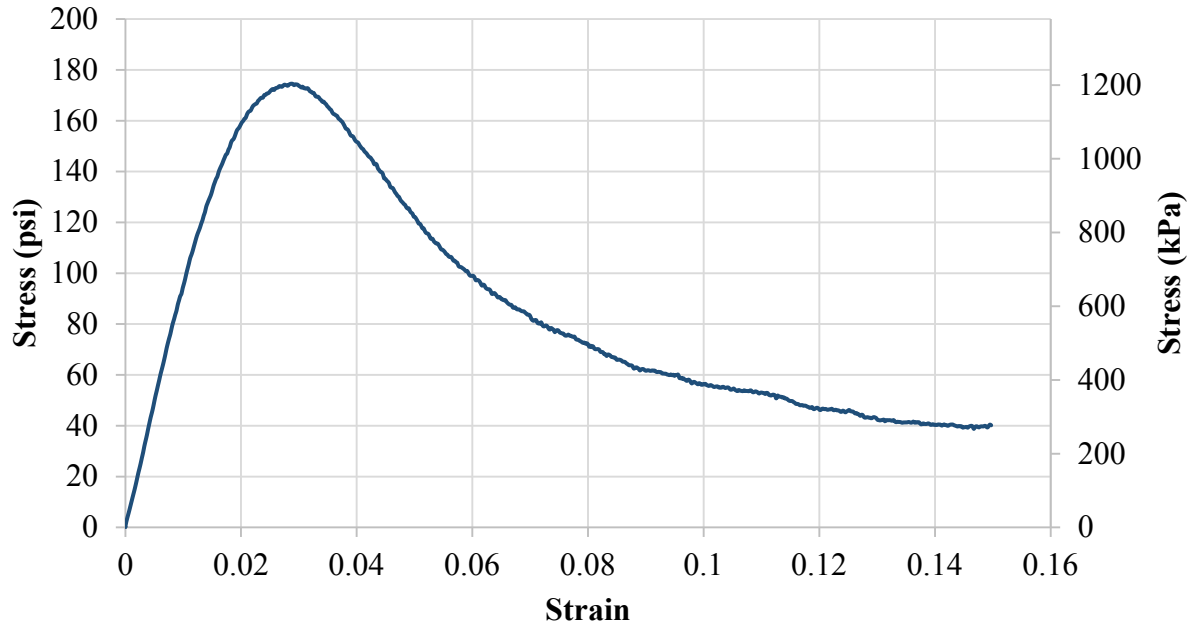

(a)

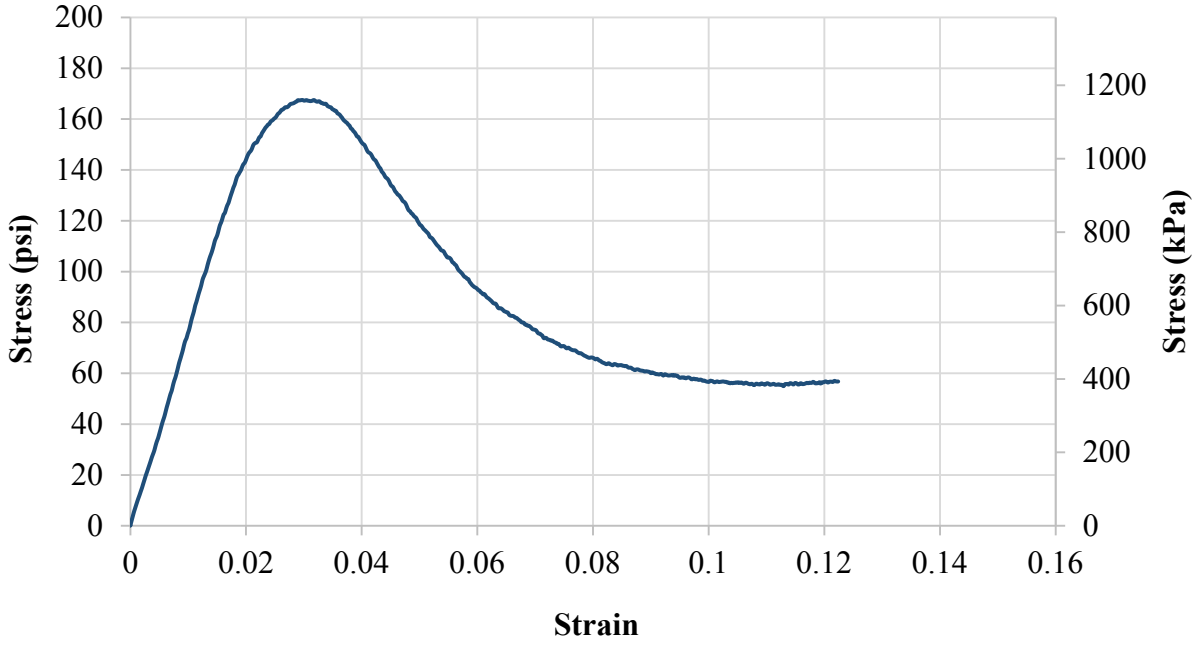

(b)

Figure B-5: Stress-strain plot for Orem base material stabilized with geogrid product D: (a) specimen 1 and (b) specimen 2.

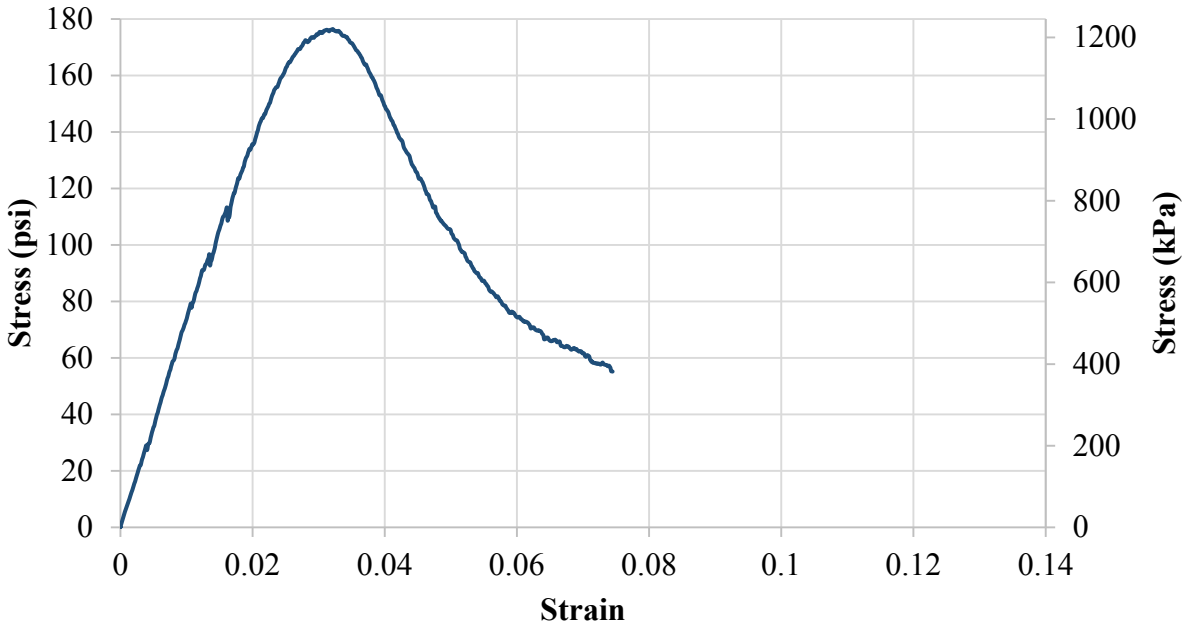

(a)

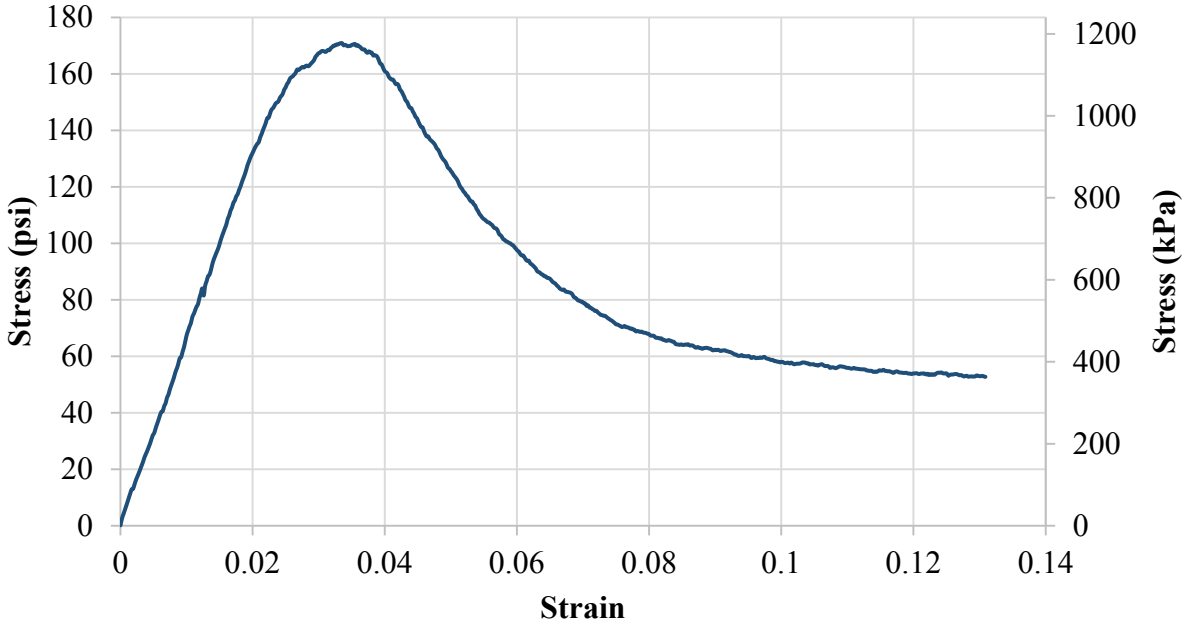

(b)

Figure B-6: Stress-strain plot for Orem base material stabilized with geogrid product E: (a) specimen 1 and (b) specimen 2.

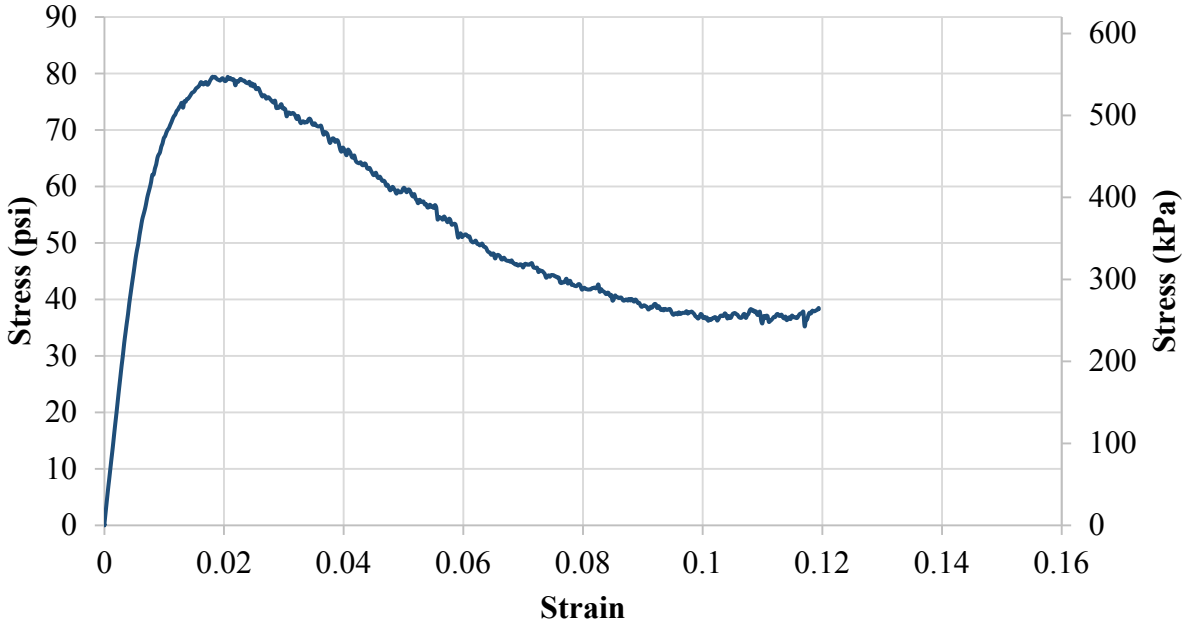

(a)

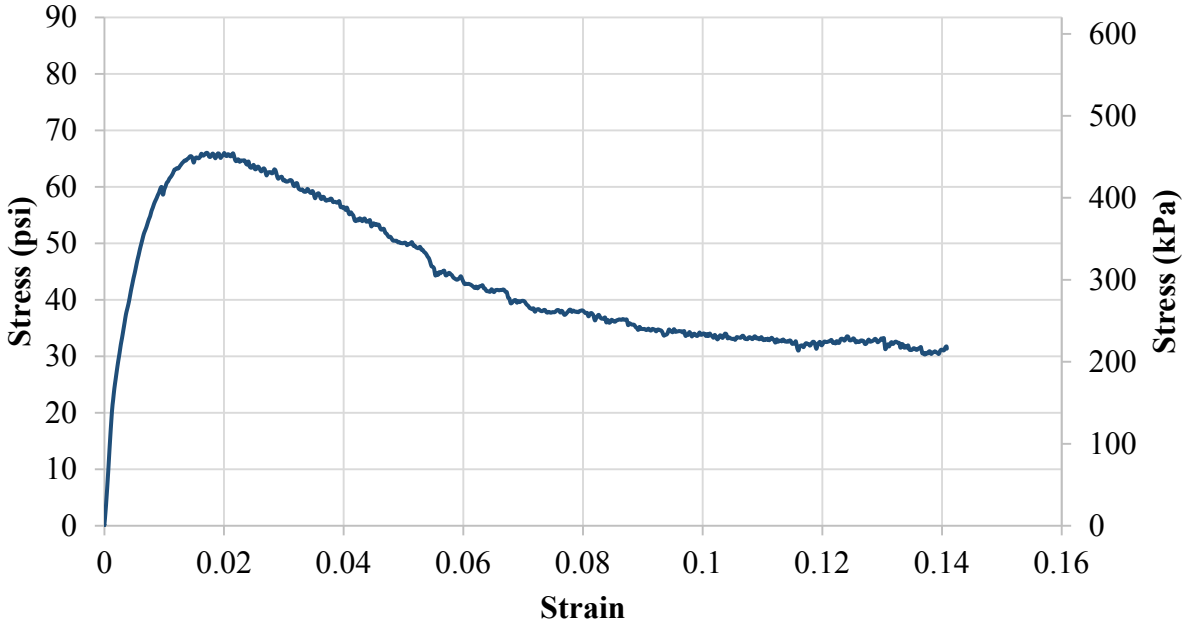

(b)

Figure B-7: Stress-strain plot for unstabilized Springville base material: (a) specimen 1 and (b) specimen 2.

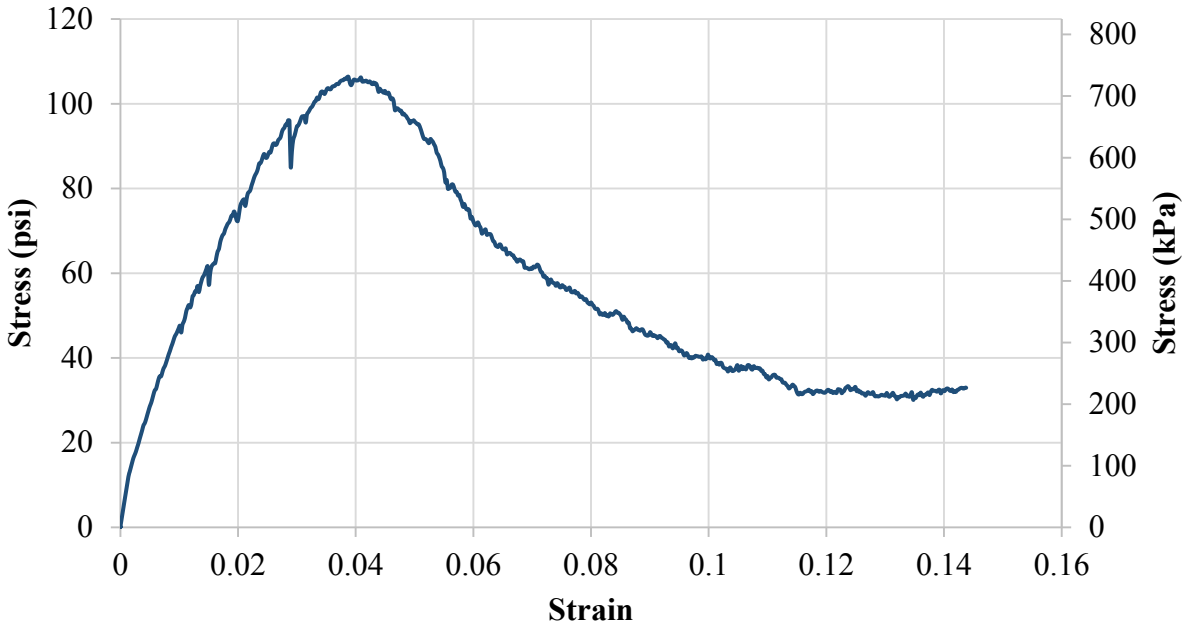

(a)

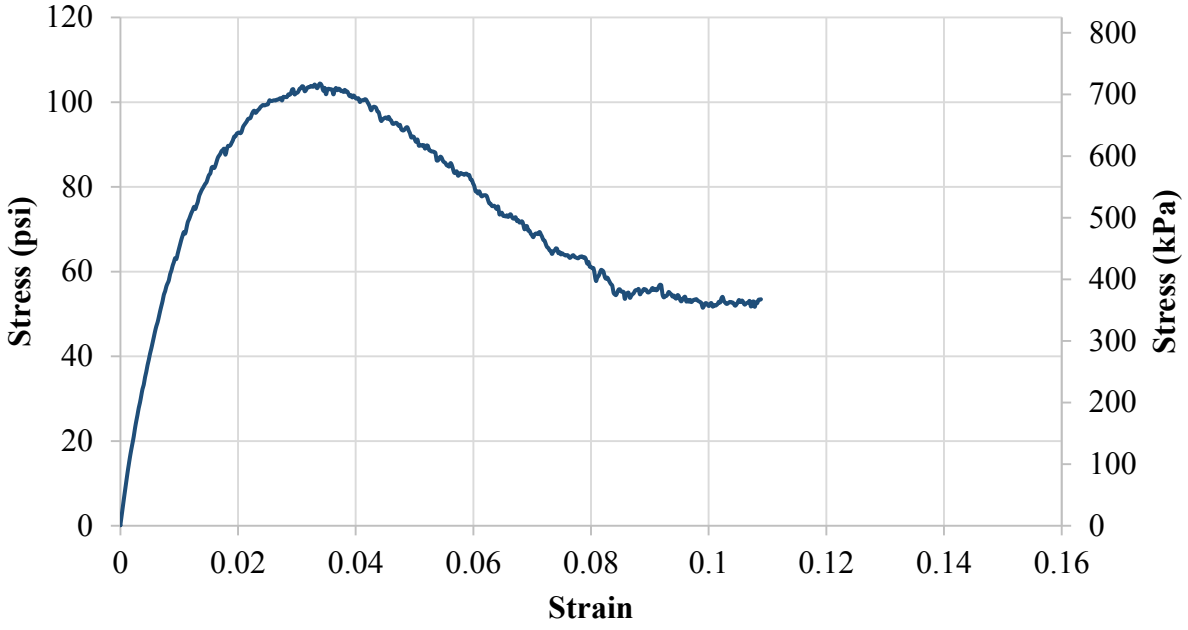

(b)

Figure B-8: Stress-strain plot for Springville base material stabilized with geogrid product A: (a) specimen 1 and (b) specimen 2.

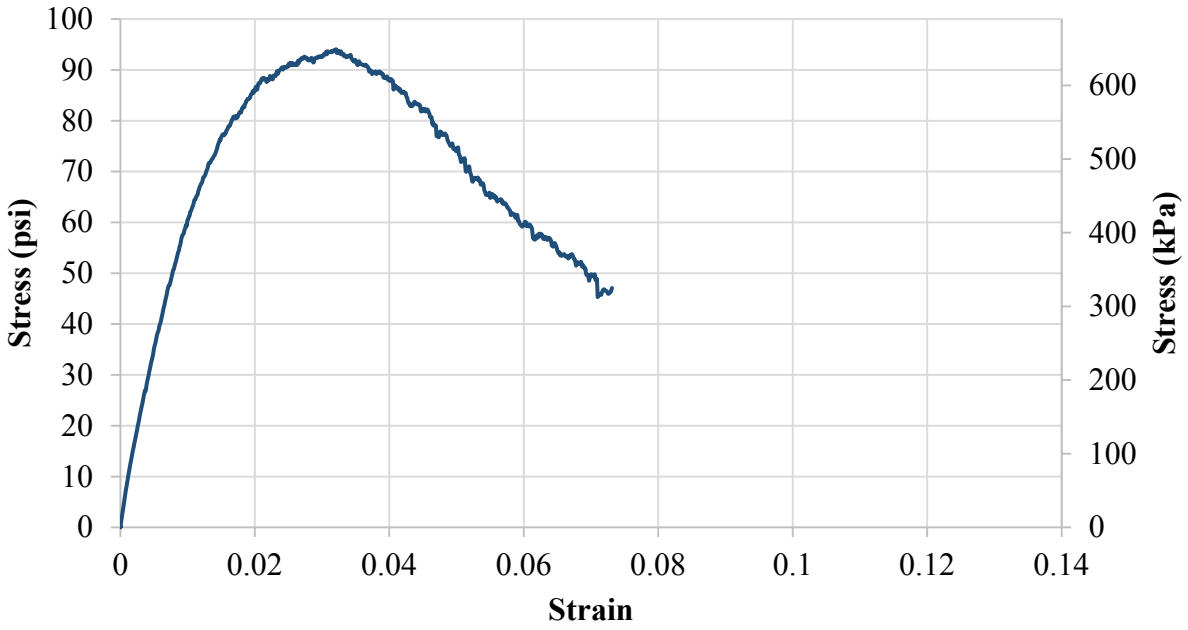

(a)

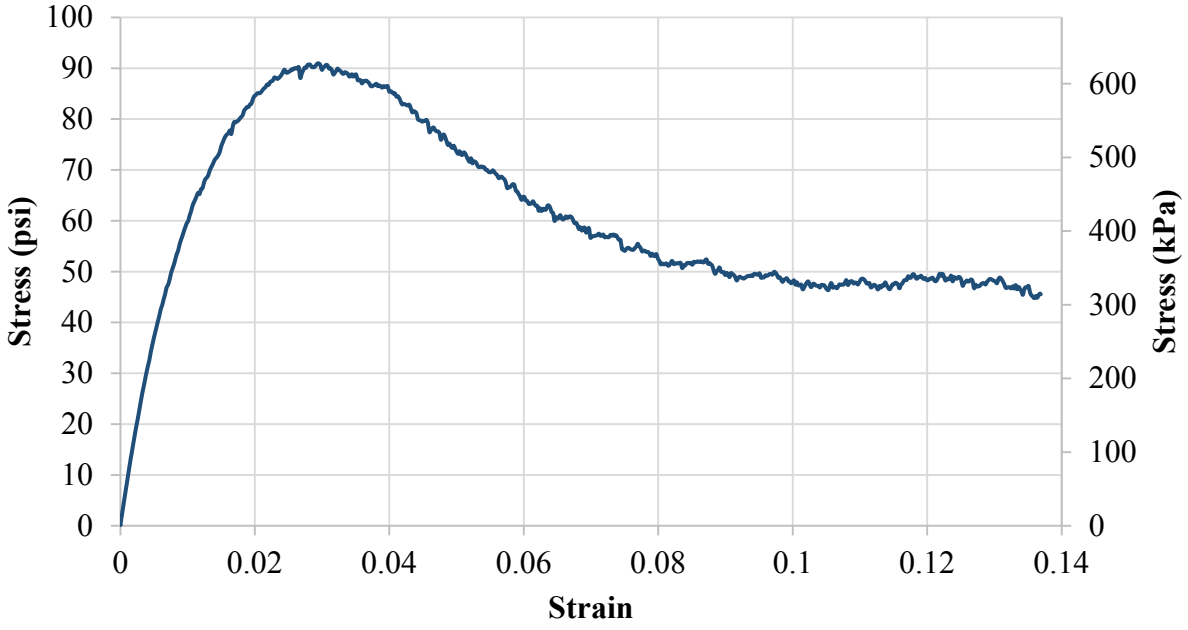

(b)

Figure B-9: Stress-strain plot for Springville base material stabilized with geogrid product B: (a) specimen 1 and (b) specimen 2.

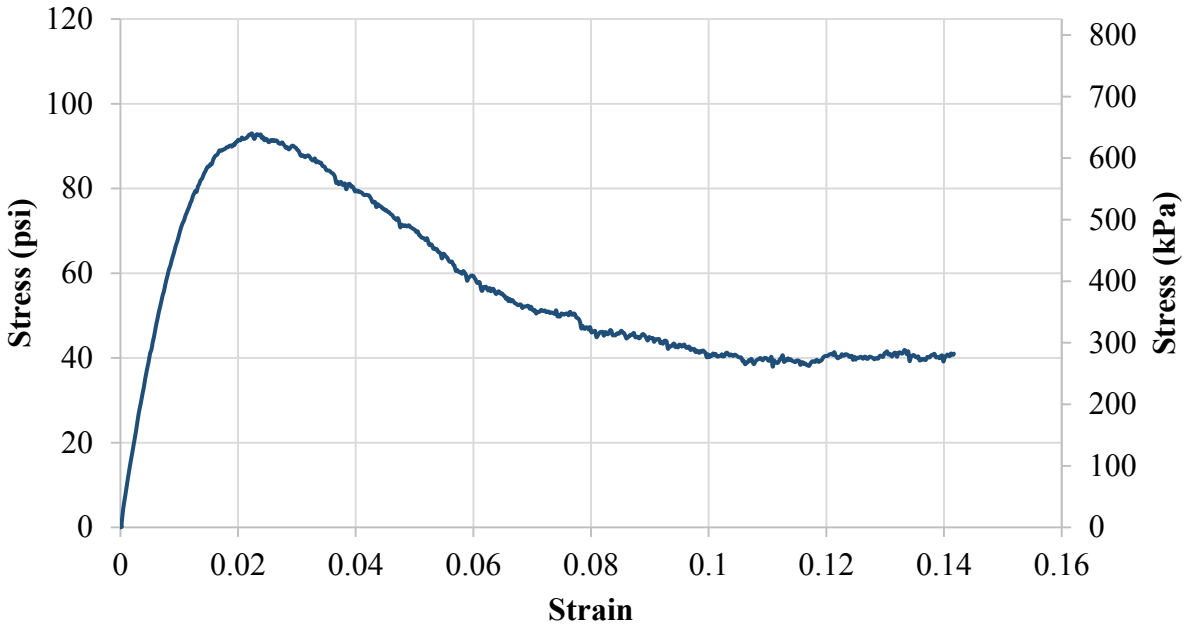

(a)

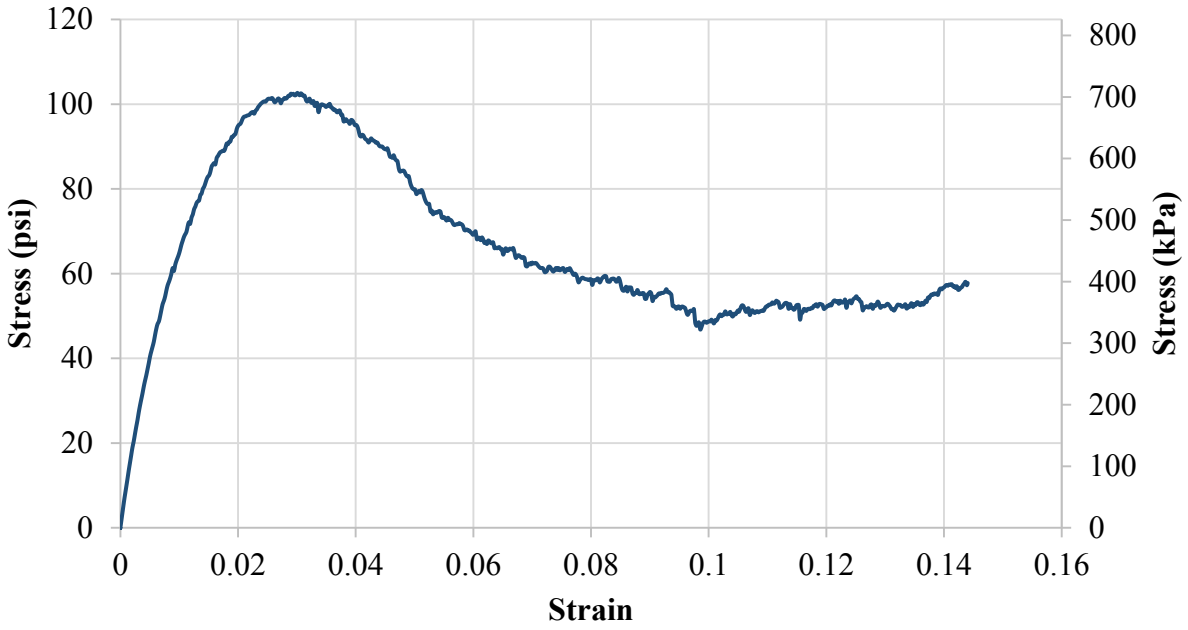

(b)

Figure B-10: Stress-strain plot for Springville base material stabilized with geogrid product C: (a) specimen 1 and (b) specimen 2.

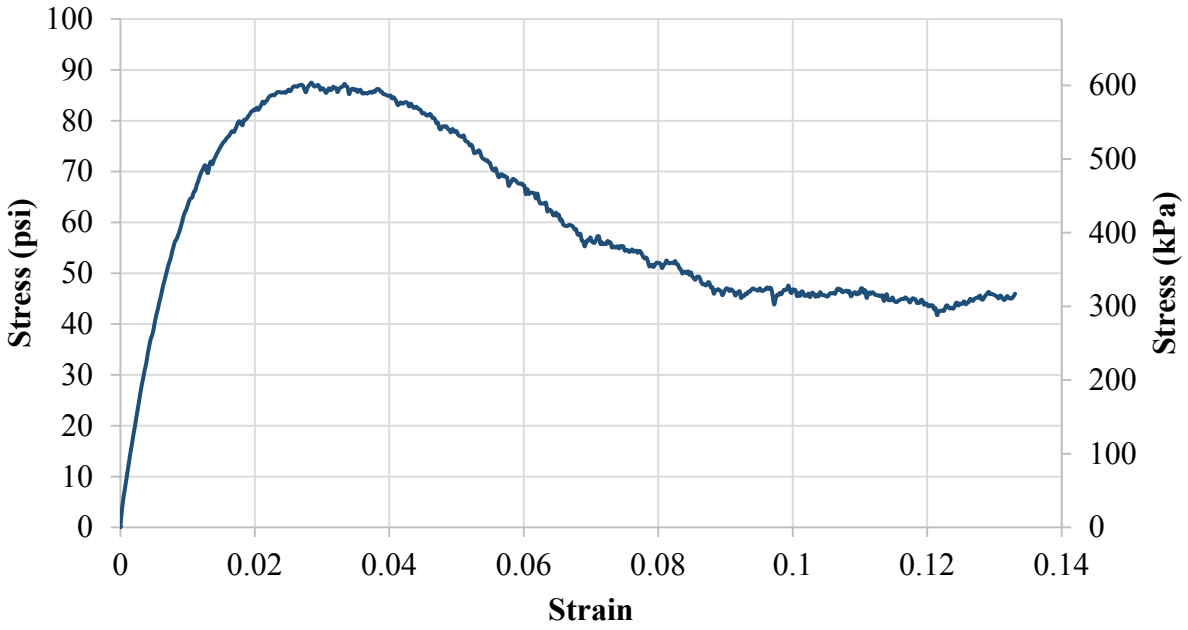

(a)

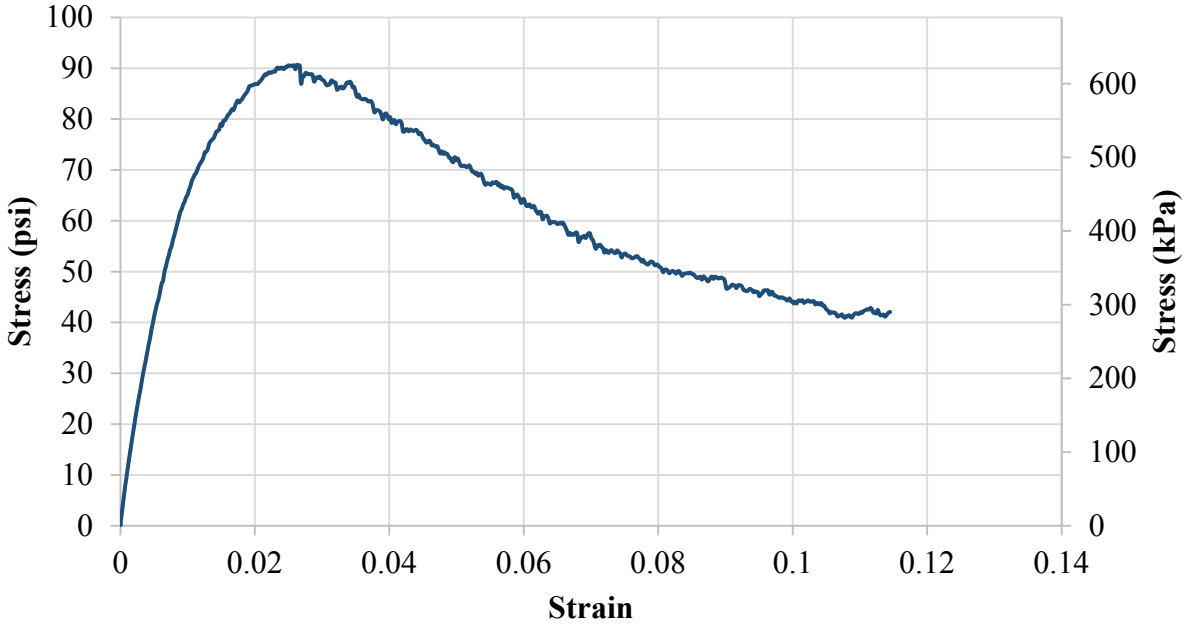

(b)

Figure B-11: Stress-strain plot for Springville base material stabilized with geogrid product D: (a) specimen 1 and (b) specimen 2.

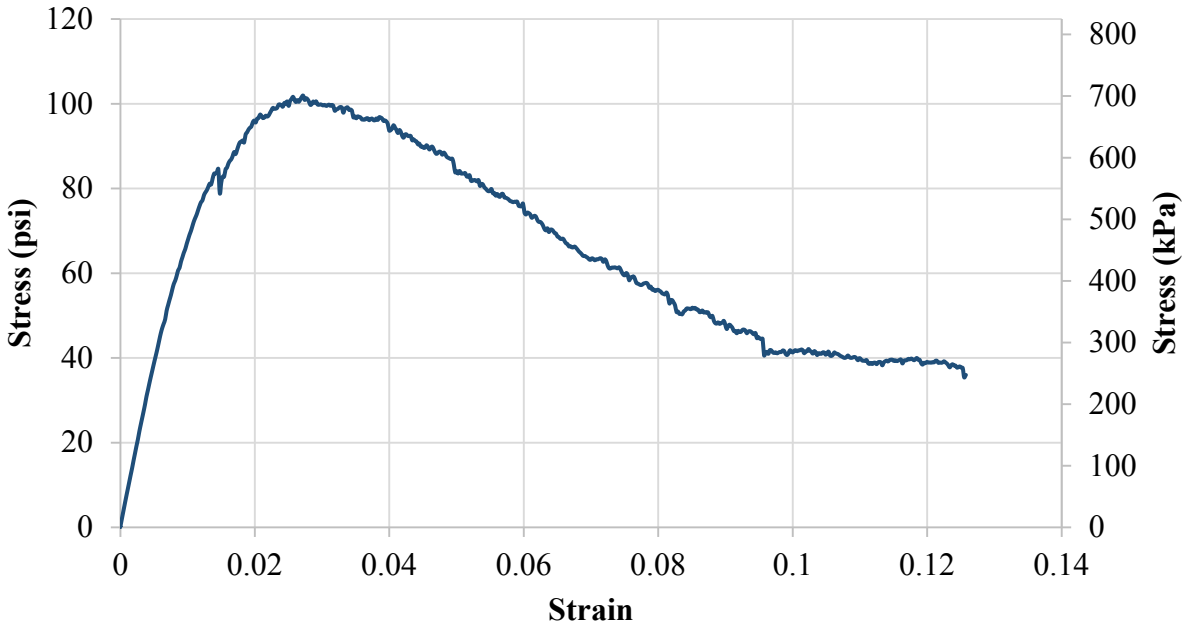

(a)

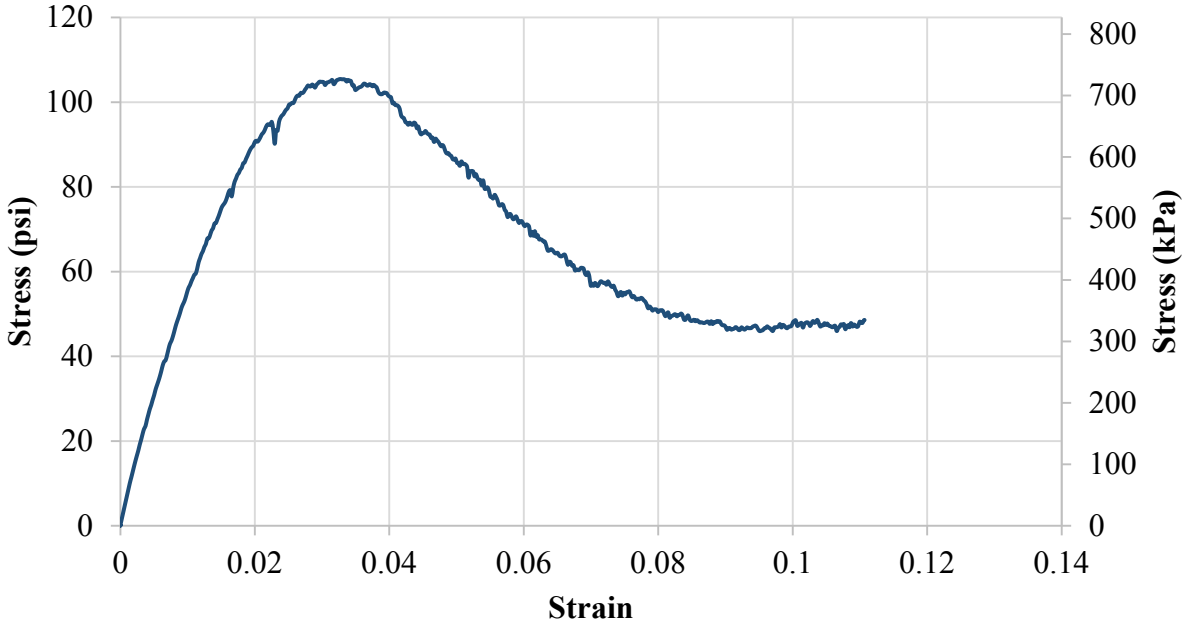

(b)

Figure B-12: Stress-strain plot for Springville base material stabilized with geogrid product E: (a) specimen 1 and (b) specimen 2.

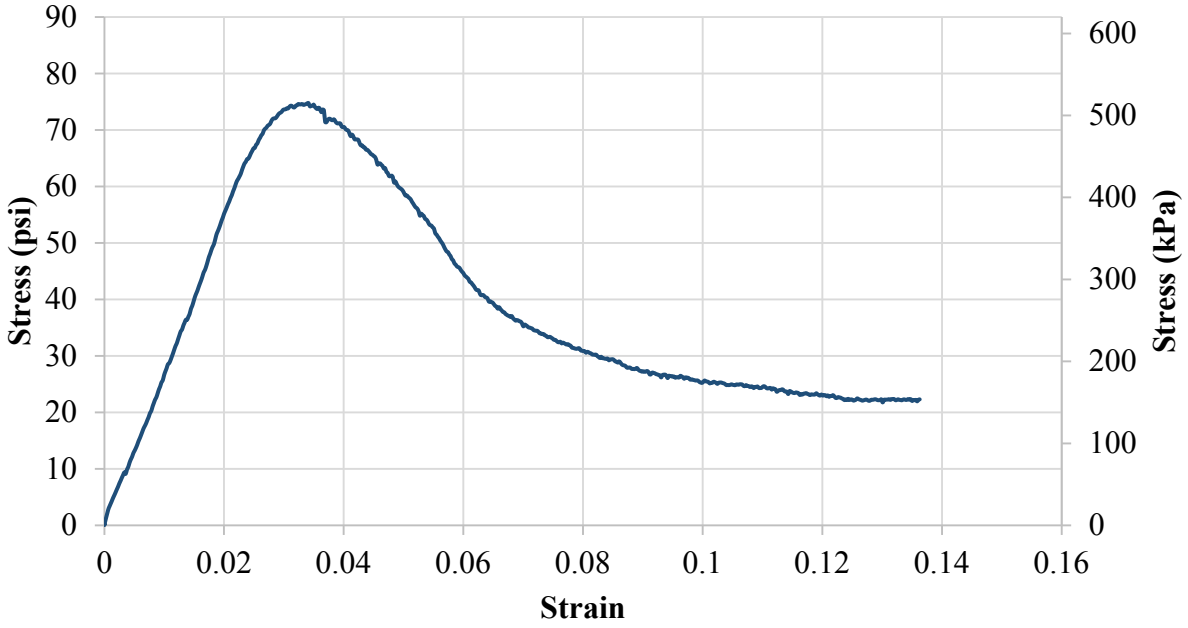

(a)

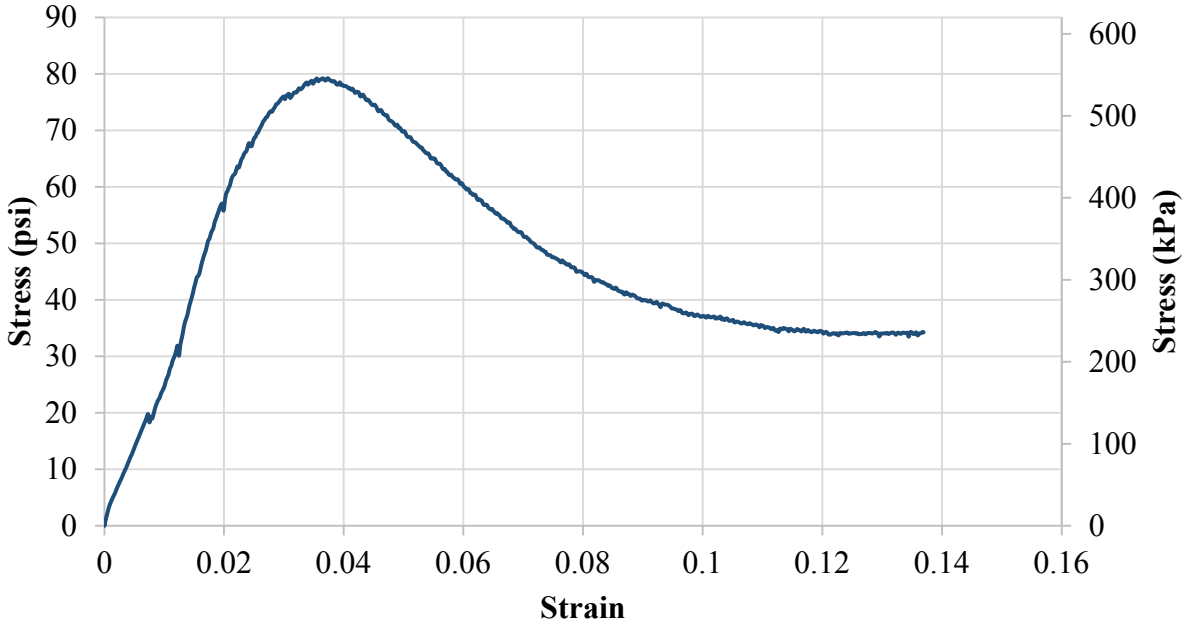

(b)

Figure B-13: Stress-strain plot for unstabilized Wells Draw Road base material: (a) specimen 1 and (b) specimen 2.

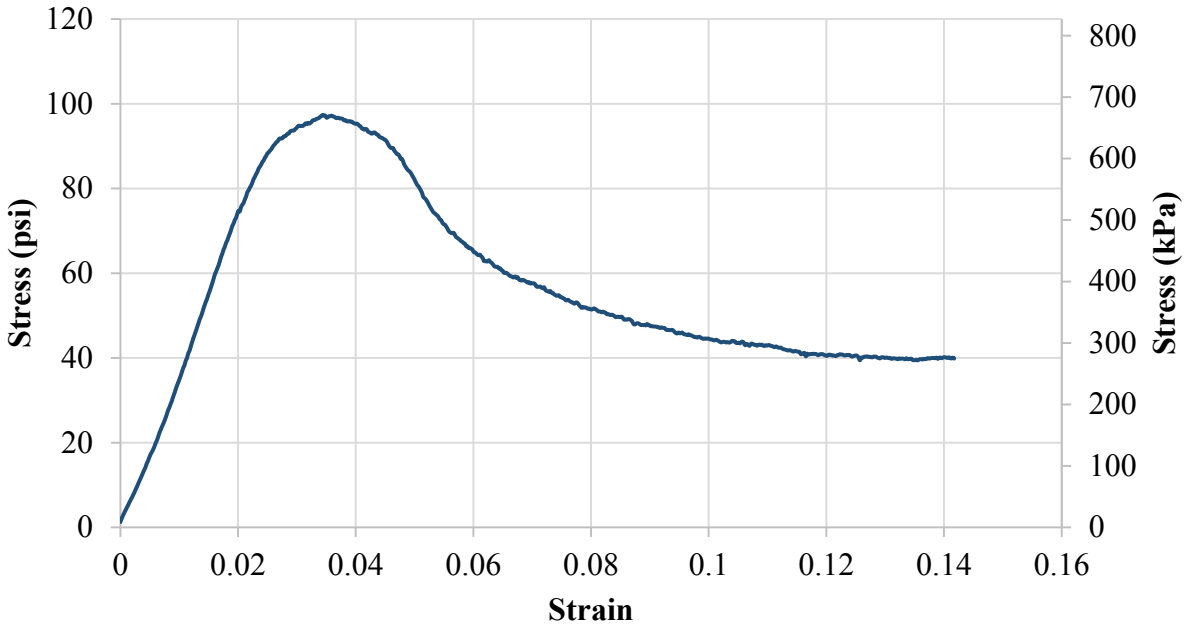

(a)

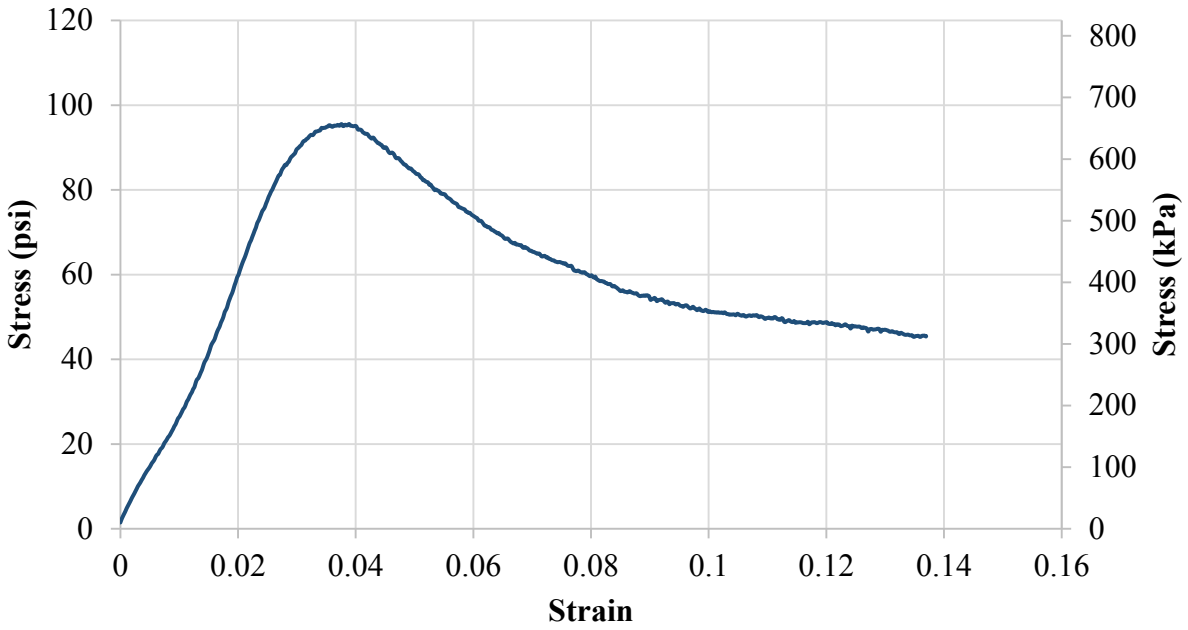

(b)

Figure B-14: Stress-strain plot for Wells Draw Road base material stabilized with a single layer of geogrid product B: (a) specimen 1 and (b) specimen 2.

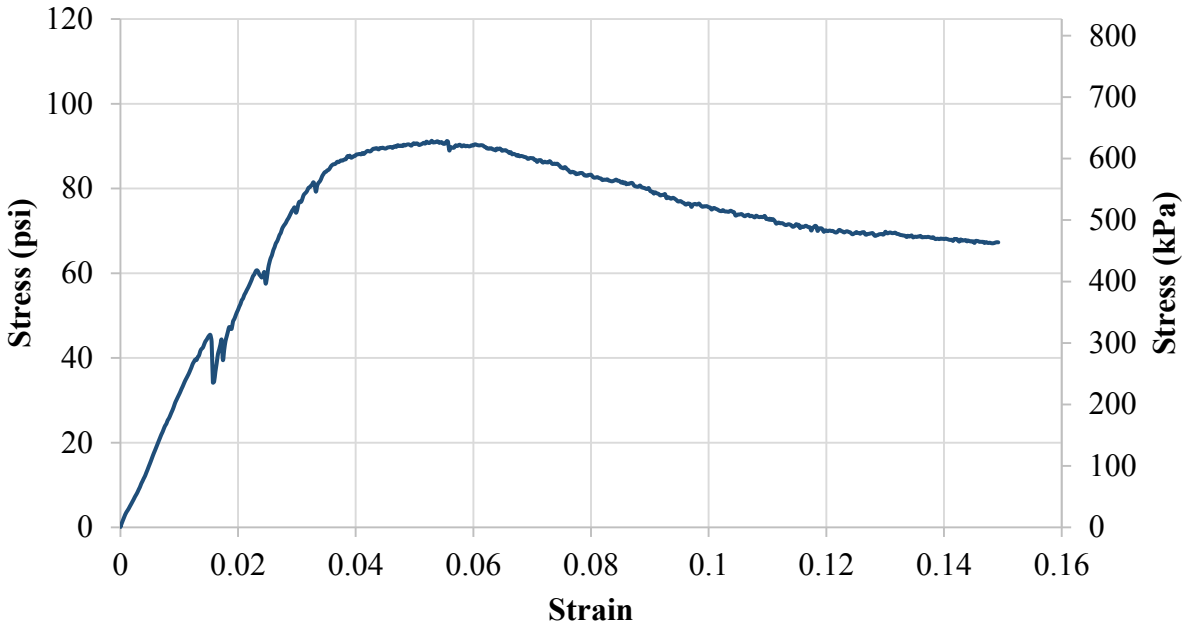

(a)

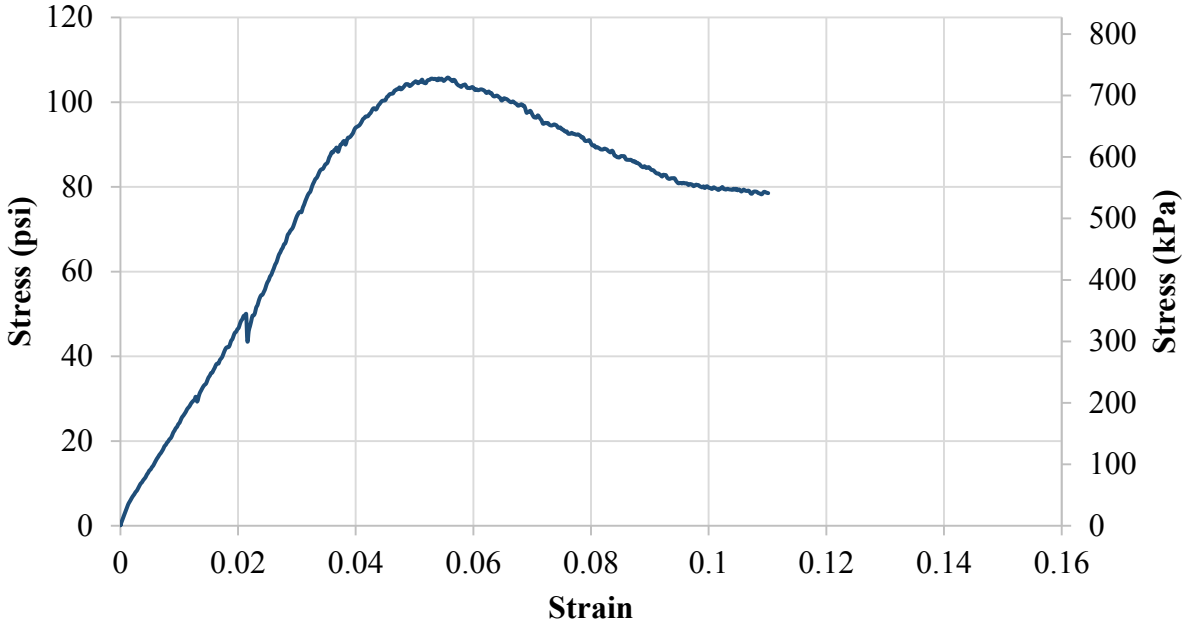

(b)

Figure B-15: Stress-strain plot for Wells Draw Road base material stabilized with a double layer of geogrid product B: (a) specimen 1 and (b) specimen 2.

APPENDIX C POST-TESTING PHOTOGRAPHS

(a)

(b)

Figure C-1: Unstabilized Orem base material: (a) specimen 1 and (b) specimen 2.

(a)

(b)

Figure C-2: Orem base material stabilized with geogrid product A: (a) specimen 1 and (b) specimen 2.

(a)

(b)

Figure C-3: Orem base material stabilized with geogrid product B: (a) specimen 1 and (b) specimen 2.

(a)

(b)

Figure C-4: Orem base material stabilized with geogrid product C: (a) specimen 1 and (b) specimen 2.

(a)

(b)

Figure C-5: Orem base material stabilized with geogrid product D: (a) specimen 1 and (b) specimen 2.

(a)

(b)

Figure C-6: Orem base material stabilized with geogrid product E: (a) specimen 1 and (b) specimen 2.

(a)

(b)

Figure C-7: Unstabilized Springville base material: (a) specimen 1 and (b) specimen 2.

(a)

(b)

Figure C-8: Springville base material stabilized with geogrid product A: (a) specimen 1 and (b) specimen 2.

(a)

(b)

Figure C-9: Springville base material stabilized with geogrid product B: (a) specimen 1 and (b) specimen 2.

(a)

(b)

Figure C-10: Springville base material stabilized with geogrid product C: (a) specimen 1 and (b) specimen 2.

(a)

(b)

Figure C-11: Springville base material stabilized with geogrid product D: (a) specimen 1 and (b) specimen 2.

(a)

(b)

Figure C-12: Springville base material stabilized with geogrid product E: (a) specimen 1 and (b) specimen 2.

(a)

(b)

Figure C-13: Unstabilized Wells Draw Road base material: (a) specimen 1 and (b) specimen 2.

(a)

(b)

Figure C-14: Wells Draw Road base material stabilized with a single layer of geogrid product B: (a) specimen 1 and (b) specimen 2.

(a)

(b)

Figure C-15: Wells Draw Road base material stabilized with a double layer of geogrid product B: (a) specimen 1 and (b) specimen 2.

(a)

(b)

Figure C-16: Omitted specimens: (a) Orem base material stabilized with geogrid product B, (b) Springville base material stabilized with geogrid product E, and (c) Wells Draw Road base material stabilized with a double layer of geogrid product B.

(c)

Figure C-16: Omitted specimens: (a) Orem base material stabilized with geogrid product B, (b) Springville base material stabilized with geogrid product E, and (c) Wells Draw Road base material stabilized with a double layer of geogrid product B, continued.

APPENDIX D ANOVA RESULTS

Table D-1: Final ANOVA Model for Geogrid Stabilization

Material	Quick Shear Test Result	*p* -values			R^2
		Geogrid Stabilization	Moisture Content	Dry Density	
Orem	Peak Axial Stress	0.000	-	-	0.7555
	Modulus to Peak Stress	0.159	-	-	0.1882
	Elastic Modulus	0.159	-	-	0.1883
	Modulus at 2% Strain	0.131	-	-	0.2128
Springville	Peak Axial Stress	0.001	-	-	0.6556
	Modulus to Peak Stress	0.027	-	0.039	0.6573
	Elastic Modulus	0.038	-	0.047	0.6270
	Modulus at 2% Strain	0.024	-	-	0.4139
Wells Draw Road	Peak Axial Stress	0.001	-	0.018	0.9793
	Modulus to Peak Stress	0.889	-	-	0.0055
	Elastic Modulus	0.863	-	-	0.0083
	Modulus at 2% Strain	0.886	-	-	0.0058

Table D-2: Final ANOVA Model for Geogrid Product or Configuration

Material	Quick Shear Test Result	*p* -values			R^2
		Geogrid Product or Configuration	Moisture Content	Dry Density	
Orem	Peak Axial Stress	0.000	-	-	0.9683
	Modulus to Peak Stress	0.163	-	-	0.6623
	Elastic Modulus	0.156	-	-	0.6684
	Modulus at 2% Strain	0.009	-	-	0.8855
Springville	Peak Axial Stress	0.005	-	-	0.9026
	Modulus to Peak Stress	0.050	-	-	0.7850
	Elastic Modulus	0.069	-	-	0.7573
	Modulus at 2% Strain	0.137	-	-	0.6849
Wells Draw Road	Peak Axial Stress	0.014	-	0.041	0.9863
	Modulus to Peak Stress	0.013	0.025	0.049	0.9999
	Elastic Modulus	0.037	-	-	0.8895
	Modulus at 2% Strain	0.119	-	-	0.7580

Table D-3: Results of Tukey's Method for Peak Axial Stress for Orem Material

Geogrid Product	*p* -values				
	A	B	C	D	E
None	**0.0001**	**0.0058**	**0.0005**	**0.0012**	**0.0008**
A		**0.0065**	0.2951	0.0519	0.0985
B			0.0626	0.3558	0.1869
C				0.6391	0.9072
D					0.9881

Table D-4: Results of Tukey's Method for Modulus to Peak Stress for Orem Material

Geogrid Product	*p* -values				
	A	B	C	D	E
None	1.0000	0.2526	0.9339	0.8325	0.2877
A		0.2821	0.9581	0.8740	0.3208
B			0.6182	0.7613	1.0000
C				0.9996	0.6791
D					0.8172

Table D-5: Results of Tukey's Method for Elastic Modulus for Orem Material

Geogrid Product	*p* -values				
	A	B	C	D	E
None	1.0000	0.2270	0.9440	0.7782	0.3154
A		0.2466	0.9607	0.8132	0.3416
B			0.5501	0.7719	0.9995
C				0.9968	0.7028
D					0.8989

Table D-6: Results of Tukey's Method for Modulus at 2 Percent Strain for Orem Material

Geogrid Product	*p* -values				
	A	B	C	D	E
None	**0.0141**	0.9735	0.1024	0.0889	0.9999
A		**0.0279**	0.4629	0.5225	**0.0170**
B			0.2268	0.1967	0.9936
C				1.0000	0.1277
D					0.1107

Table D-7: Results of Tukey's Method for Peak Axial Stress for Springville Material

Geogrid Product	*p* -values				
	A	B	C	D	E
None	**0.0051**	0.0546	**0.0188**	0.1137	**0.0067**
A		0.2460	0.6853	0.1162	0.9992
B			0.8839	0.9792	0.3514
C				0.5640	0.8432
D					0.1682

Table D-8: Results of Tukey's Method for Modulus to Peak Stress for Springville Material

Geogrid Product	*p* -values				
	A	B	C	D	E
None	0.0576	0.0740	0.8123	0.1751	0.4443
A		0.9998	0.2235	0.9001	0.4933
B			0.2886	0.9625	0.6073
C				0.6177	0.9663
D					0.9430

Table D-9: Results of Tukey's Method for Elastic Modulus for Springville Material

Geogrid Product	*p* -values				
	A	B	C	D	E
None	0.0773	0.1082	0.8986	0.2447	0.4761
A		0.9994	0.2385	0.8904	0.5906
B			0.3322	0.9705	0.7456
C				0.6618	0.9345
D					0.9835

Table D-10: Results of Tukey's Method for Modulus at 2 Percent Strain for Springville Material

Geogrid Product	*p* -values				
	A	B	C	D	E
None	0.6996	0.5765	0.1519	0.6136	0.1273
A		0.9998	0.6711	1.0000	0.5908
B			0.7913	1.0000	0.7141
C				0.7559	1.0000
D					0.6766

Table D-11: Results of Tukey's Method for Peak Axial Stress for Wells Draw Road Material

Geogrid Product	*p* -values	
	B (Single)	B (Double)
None	**0.0178**	**0.0150**
B (Single)		0.6397

Table D-12: Results of Tukey's Method for Modulus to Peak Stress for Wells Draw Road Material

Geogrid Product	*p* -values	
	B (Single)	B (Double)
None	**0.0176**	**0.0289**
B (Single)		**0.0122**

Table D-13: Results of Tukey's Method for Elastic Modulus for Wells Draw Road Material

Geogrid Product	*p* -values	
	B (Single)	B (Double)
None	0.1260	0.2513
B (Single)		**0.0330**

Table D-14: Results of Tukey's Method for Modulus to 2 Percent Strain for Wells Draw Road Material

Geogrid Product	*p* -values	
	B (Single)	B (Double)
None	0.3215	0.4874
B (Single)		0.1082